Available online at www.sciencedirect.com
ScienceDirect
Fluid Dynamics Research 40 (2008) 695–736
FLUID DYNAMICS RESEARCH

Chaotic advection and nonlinear resonances in an oceanic flow above submerged obstacle

K.V. Koshel[a,*], M.A. Sokolovskiy[b,c], P.A. Davies[d]

[a] *Pacific Oceanological Institute of FEB RAS, 43, Baltiyskaya Str., 690041, Vladivostok, Russia*
[b] *Water Problems Institute of RAS, 3, Gubkina Str., 119333, Moscow, Russia*
[c] *Institute of Mathematics and Mechanics of UB RAS, 16, Kovalevskaya Str., Ekaterinburg 620219, Russia*
[d] *Department of Civil Engineering, The University, Dundee DD1 4HN, UK*

Received 30 October 2007; received in revised form 12 March 2008; accepted 14 March 2008
Available online 11 April 2008
Communicated by A.D. Gilbert

Abstract

The effect of an isolated submarine obstacle on the motion of fluid particles in a periodic external flow is studied within the framework of the barotropic, quasi-geostrophic approximation on f-plane. The concept of background currents advanced by Kozlov [1995. Background currents in geophysical hydrodynamics. Izvestia, Atmos. Oceanic Phys. 31 (2), 245–250] is used to construct a dynamically consistent stream function satisfying the potential vorticity conservation law. It is shown that a system of two topographic vortices revolving about a rotation center can form in a circular external flow. Unsteady periodic perturbations, associated with either variations in the background current or deviations of the external flow from circulation, are analyzed. Unsteadiness in the external flow essentially complicates the pattern of the motion of fluid particles. Vortex-type quasi-periodic structures, identified with nonlinear resonances that form in Lagrangian equations of fluid particle advection, are examined. They either surround the stationary configuration by a vortex chain—a ringlet-like structure [Kennelly, M.A., Evans, R.H., Joyce, T.M., 1985. Small-scale cyclones on the periphery of Gulf Stream warm-core rings. J. Geophys. Res. 90(5), 8845–8857], or they form a complex-structure multivortex domain. Asymptotic estimates and numerical modeling are used to study the distribution and widths of the nonlinear resonance domains that appear under unsteady perturbations of different types. The onset of chaotic regimes owing to the overlapping of nonlinear resonance domains is analyzed. Transport fluxes determined by chaotic advection and barriers for transport

* Corresponding author. Tel.: +7 4232444012; fax: +7 4232312573.
E-mail address: kvkoshel@poi.dvo.ru (K.V. Koshel).

doi:10.1016/j.fluiddyn.2008.03.001

(KAM-tori) and the conditions of their existence are studied. The relation of the rotation frequency of fluid particles on their initial position (when the dependence is calculated in the undisturbed system) is shown to completely determine the main features of the pattern of Lagrangian trajectories and chaotization effects. Because of nonlinear effects, the domain involved in quasi-periodic and chaotic motions can be much larger than the domain occupied by steady topographic vortices. The results of study by Sokolovskiy et al. [1988. On the influence of an isolated submerged obstacle on a barotropic tidal flow. Geophys. Astrophys. Fluid Dyn. 88(1), 1–30] concerning the due regard on the irrotational background component as the necessary factor for the transportation of fluid particles from the vortex domain to infinity are confirmed.

PACS: 05.45.−a; 05.45.Pq; 74.30.Jj; 47.52.+j

Keywords: Chaotic advection; Nonlinear resonances; Quasi-geostrophic flows

0. Introduction

Notwithstanding the fact that the property of mixing of trajectories that initially were close to one another, which is known now as *chaotic advection* (Aref, 1984,2002), in unsteady regular geophysical flows was mentioned by Eckart (1948) almost 60 years ago and later demonstrated by Welander (1955), systematic studies of chaotic advection in the atmosphere, natural estuaries and oceans began only four decades later. Significant results have been obtained in this field in the recent 15 years. We give here a brief list of a relatively small number of studies, which, one way or another, relate to the problems of geophysical hydrodynamics. A more detail description of these problems can be found, for example, in reviews (Zeng et al., 1993; Wiggins, 2005; Mancho et al., 2004, 2006).

Pierrehumbert (1991a, b) used estimates of Lyapunov indices, calculated within a finite time interval,[1] to prove the existence of chaotic mixing in atmospheric Rossby waves in the presence of small periodic perturbations. The chaotic properties of a dynamo were established with the use of such a method by Llewellyn Smith and Tobias (2004).

The teleconnection between oceanic surface temperature anomalies in the equatorial part of the Pacific and the atmospheric activity in the middle and northern latitudes, a phenomenon discovered by Bjerknes (1966, 1969), was further described by the model of atmospheric blocking, interpreted as a result of synchronization of chaos in different parts of the ocean (Duane, 1977; Duane et al., 1999; Duane and Tribbia, 2001, 2004).

The nonlinear stability of the dynamic system of equations describing the motion of fluid particles along trajectories associated with a meandering jet was analyzed by Samelson (1992) with the use of Melnikov's method. He found the conditions, depending on kinematic parameters, for splitting of separatrices in the phase portrait. These results provide an explanation for the motion of the fluid particles that cross the jet flow. Thus, the question "The Gulf Stream—barrier or blender?" (Bower et al., 1985) was given the answer: "both—a barrier and a blender". These results were generalized to the case of time and scale variations in the jet stream in Bower (1991), del-Castillo-Negrete and Morrison (1993), Meyers (1994), Duan and Wiggins (1996), Rogerson et al. (1999), and Wiggins (2005). Melnikov's method, a reliable

[1] A physical explanation of the choice of a finite time interval is given by Yang (1993a, b) and Poje and Haller (1999).

tool for the identification of chaotic trajectories, was successfully used also by Allen et al. (1991), Simiu (1969) for studying drift coastal currents, by Malhotra and Wiggins (1998) in their studies of Rossby waves, and by Balasuriya and Jones (2001) for studying the diffusion of a mesoscale vortex.

The problem of kinematic barriers, which are identified with KAM-tori of the respective dynamic systems, has been discussed (Yang, 1993b, 1996c, 1998; Cox et al., 1990; Ngan and Shepherd, 1997) in the context of the interaction between a jet stream and a Rossby wave, and in studies (Yang, 1996a, b; Yang and Liu, 1994, 1997; Liu and Yang, 1994) applied to the contact zone between two large oceanic vortices. Similar transport barriers are stratospheric polar vortices, which, like a containment vessel, separate the external surf zone, where the potential vortex distribution is uniform, from the internal zone, where mixing is much weaker. This problem was discussed from the viewpoint of chaotic dynamics in several works (Yang, 1993b; Pierce and Fairlie, 1993; Pierce et al., 1994; Ngan Shepherd, 1999a, b; Mizuta and Yoden, 2001; Coulliette and Wiggins, 2001; Koh and Legras, 2002; Prants et al., 2006; Koshel and Prants, 2006).

The formation processes of chaotic transport and mixing of tracers in the unsteady motion of vortices are studied in works Neu (1984), Polvani and Wisdom (1990), Polvani and Plumb (1992), Meleshko et al. (1992), Meleshko and Konstantinov (1993), Babiano et al. (1994), Velasco Fuentes (1994), Velasco Fuentes et al. (1995), Péntek et al. (1995), Boffetta et al. (1996), Kuznetsov and Zaslavsky (1998, 2000), Friedland (1999), Kawakami and Funakoshi (1999), von Handerberg et al. (2000), Bracco et al. (2000), Leoncini et al. (2000, 2001), Leoncini and Zaslavsky (2002), Abraham and Bowen (2002), Angilella and Brancher (2003), Vilela et al. (2006).

The chaotic dynamics of the vortex-flow system was studied in Yatsuyanagi et al. (2001), Waseda and Mitsudera (2002), and Gudimenko (2007). Analysis of hyperbolic trajectories is used in Kuznetsov et al. (2002) to study the transport properties of particles in the vicinity of an oceanic ring in the Gulf of Mexico. In the paper by Miller et al. (2002), where lobe analysis method is used to study an unsteady recirculation flow captured by an island shore, a relationship was found to exist between the chaotic transport of particles and surface Ekman pumping. Radical distinctions between the regular behavior of trajectories in the core of the Antarctic Circumpolar Current and the chaotic behavior of trajectories at its periphery were mentioned by Nycander et al. (2002).

The chaotic motion of point geostrophic vortices is discussed in Novikov (1975), Novikov and Sedov (1978), Aref and Pomphrey (1982), Eckhardt and Aref (1988), Meleshko and Konstantinov (1993), Marshall (1995), Borisov and Mamaev (2005), Borisov et al. (2005), Gryanik et al. (2006) and Gudimenko (2007).

Aref's guess (1984, 1990) that chaotic phenomena should take place in tidal oceanic currents was confirmed by a vast body of data in subsequent studies (Pasmanter, 1991; Ridderinkhof and Zimmerman, 1992; Ridderinkhof and Loder, 1994; Paldor and Boss, 1994; Beerens et al., 1994; Stolovitsky et al., 1995; Loder et al., 1997; de Swart et al., 1997; Maas and Doelman, 2002; Stirling, 2003; Sakamoto and Akitomo, 2006).

Much attention was given to studies of chaotic mixing in unsteady oceanic and atmospheric flows over irregularities in the underlying surface (Allen et al., 1991; Ridderinkhof and Loder, 1994; Goldner and Chapman, 1997; Kozlov and Koshel, 1999, 2000, 2001, 2003; Wåhlin, 2004; Izrailsky et al., 2004; Grote, 1999; Budyansky et al., 2002, 2004a, b, 2007; Koshel and Stepanov, 2005, 2006a, b; Izrailsky et al., 2006), including those above the continental shelf (Samelson and Allen, 1987; Kuebel Cervantes et al., 2004).

In this study, we discuss the possible regular and chaotic regimes in the problem of a quasiperiodic flow around a submarine elevation of Gaussian form.

1. Problem formulation

The generation of regular free and trapped topographic vortices as a result of interaction between an oceanic current and bed relief irregularities has been studied well (Ingersoll, 1969; Huppert and Bryan, 1976; Hart, 1979; Johnson, 1977, 1983; Kozlov, 1983; Zyryanov, 1985, 1995, 2006; Verron, 1986; Goldner and Chapman, 1997; Sokolovskiy et al., 1988). The studies of chaotic advection above submarine elevations cited in the introduction are focused, as a rule, on a unidirectional flow. However, currents with varying direction (for example, flood currents or currents that feature distinct synoptic variability) are of unquestionable interest. In this study, we will concentrate most attention to the analysis of the effects of chaotic mixing in such a current in the vicinity of an isolated submarine elevation.

Within the framework of the background current concept on f-plane (Kozlov, 1995), we consider a dynamically consistent model[2] of a periodic flow above an axisymmetric elevation of Gaussian form. The concept of background currents for quasigeostrophic approximation (Kozlov, 1995; Izrailsky et al., 2004), used in this study, renders possible to express the dynamically consistent stream-function $\Psi(x, y, t)$ in a closed form (in quadratures).

In the model we set the condition of flow without bottom separation (in the present case the upper interface of the bottom boundary layer plays the role of the bottom). This condition is an inviscid limit of a result of the application of the joining asymptotic expansion method to the problem with boundary layer near the bottom under the more realistic non-slip boundary condition (Kozlov, 1983).

In general, we have (Kozlov, 1983, 1995; Kozlov and Koshel, 2001; Izrailsky et al., 2004)

$$\Psi(x, y, t) = \Psi_0(x, y) + \Psi_1(x, y, t),$$

where the first term represents the planetary-topographic vortical component, and a nonvortical perturbation $\Psi_1(x, y, t)$ is due to boundary conditions. The only solution of $\nabla^2\Psi_1 = 0$ for which the velocity is bounded over a boundless plane is a spatially homogeneous flow directed at an angle θ to the x-axis, with a stream-function

$$\Psi_1 = (B\sin\theta + v_0)x - (A\cos\theta + u_0)y.$$

Below $\Psi_1(x, y, t)$ will be referred to as external flow.

Here, let consider the stream-function in the form

$$\Psi = [1 + \mu\cos(\omega_0 t + \varphi_0)][(B\sin\theta(t) + v_0)x - (A\cos\theta(t) + u_0)y] + \int_0^r V(\rho)\,\mathrm{d}\rho, \tag{1}$$

where A, B, ω_0, φ_0, u_0, v_0, μ are constants, $r = \sqrt{x^2 + y^2}$, t is the time, x and y are horizontal coordinates directed eastward and northward, respectively, $V(r)$ is the radial distribution of the azimuth velocity in the vortex induced by the elevation.

Suppose that the submarine elevation has Gaussian shape

$$h(r) = \mathrm{e}^{-\alpha r^2}, \quad \alpha > 0, \tag{2}$$

[2] In the sense meant by Polvani and Wisdom (1990), Dahleh (1992), Kozlov (1995), Ngan and Shepherd (1997), Kozlov and Koshel (1999, 2003).

Then the expression for the azimuth velocity takes the form

$$V = -\frac{\sigma}{r}\int_0^r h(\rho)\rho\,\mathrm{d}\rho = \frac{\sigma}{2\alpha r}(\mathrm{e}^{-\alpha r^2} - 1). \tag{3}$$

Here $\sigma = O(1)$ is a topographic parameter, and $\alpha \approx 1.256$ was chosen in accordance with the condition $\mathrm{d}V(r)/\mathrm{d}r|_{r=1} = 0$.

The characteristic horizontal scale was taken equal to the radius of the circumference $r = R$ on which the maximum azimuth velocity is attained. Suppose that the depth of the ocean is $H = 4\,\mathrm{km}$, the mean velocity is $U = 10\,\mathrm{cm/s}$ and the characteristic circulation time of a fluid particle over a circumference with unit radius is $T = 1$ day. Then, $R = 1.375\,\mathrm{km}$ and $\sigma = 3.511$, corresponding to an elevation height of 1.021 km. In the general case, the flow velocity vector (1), (3) circumscribes an ellipse shifted relatively the center of the elevation. In the absence of perturbations, when

$$A = B, \quad \mu = u_0 = v_0 = 0, \tag{4}$$

the center of rotation coincides with the submarine elevation center and the flow is a circulation (clearly, the values of A and B are the semi-axes of the kinematic ellipse along the x and y, respectively).

The analysis of the motion of fluid particles is more convenient in a coordinate system rotating with the flow. The corresponding change of variables

$$x' = x\cos\theta(t) + y\sin\theta(t),$$
$$y' = -x\sin\theta(t) + y\cos\theta(t)$$

results in the following expression for the stream-function

$$\Psi' = -Ay' + \delta\Psi(x', y', t) + \int_0^r V'(\rho)\,\mathrm{d}\rho, \tag{5}$$

where

$$V'(r) = V(r) - \dot{\theta}r. \tag{6}$$

The unsteady part of the stream-function, which we consider as a perturbation, has the form

$$\begin{aligned}\delta\Psi = &-A\mu\sin(\omega_0 t + \varphi_0)y' + [1 + \mu\sin(\omega_0 t + \varphi_0)]\{x'[(B - A)\sin\theta\cos\theta \\ &+ v_0\cos\theta - u_0\sin\theta] - y'[(B - A)\sin^2\theta + v_0\sin\theta + u_0\cos\theta]\}.\end{aligned} \tag{7}$$

In the absence of perturbations, the stream-function will be steady, and the trajectories of fluid particles will be regular. As will be shown below, any external perturbation makes the trajectories chaotic.

The equations of motion of fluid particles in a rotating coordinate system have the form

$$\begin{aligned}\frac{\mathrm{d}x'}{\mathrm{d}t} &= -\frac{\partial\Psi'}{\partial y'} = A - V'(r)\frac{y'}{r} - \frac{\partial(\delta\Psi)}{\partial y'}, \\ \frac{\mathrm{d}y'}{\mathrm{d}t} &= \frac{\partial\Psi'}{\partial x'} = V'(r)\frac{x'}{r} + \frac{\partial(\delta\Psi)}{\partial x'}.\end{aligned} \tag{8}$$

Thus, we have a Hamiltonian system with an unsteady stream-function playing the role of the Hamiltonian. The phase space in this case coincides with the configuration space. The origination of chaos in such systems is a quite common phenomenon (Brown and Samelson, 1994; Zaslavsky, 2007).

Hereinafter, we will consider an external flow rotating with a constant frequency Ω, i.e. set $\theta(t) = \Omega t$.

2. Analysis of the steady state

Suppose that conditions (4) are satisfied. In Fig. 1, where the azimuth velocity is given with the negative sign (for the sake of convenience), it can be readily seen that the motion becomes solid-body with increasing distance from the center, in the asymptotic limit (inclined dashed straight line). The profiles of both branches of the azimuth velocity each have two local extremes, though when the frequency Ω is high, a situation is possible when there will be no extreme. The same figure shows the profiles of ω—the circulation frequency of the fluid particles that originally belonged to the y-axis about the center of rotation of the undisturbed system. As was shown by Koshel and Stepanov (2006b), this function plays a key role in the qualitative study of the chaotization of phase space.

Let us detail the relationships shown in Fig. 1, where the frequency of the external circular flow Ω=0.14. Note that, with the chosen characteristic scales, this frequency corresponds to processes with a synoptic period of $T \approx 45$ days.

If the value of A lies in one of the intervals between the local extreme of function V, three singular points exist in the $x' = 0$ axis—two outer points are elliptic and an intermediate point is hyperbolic.[3]

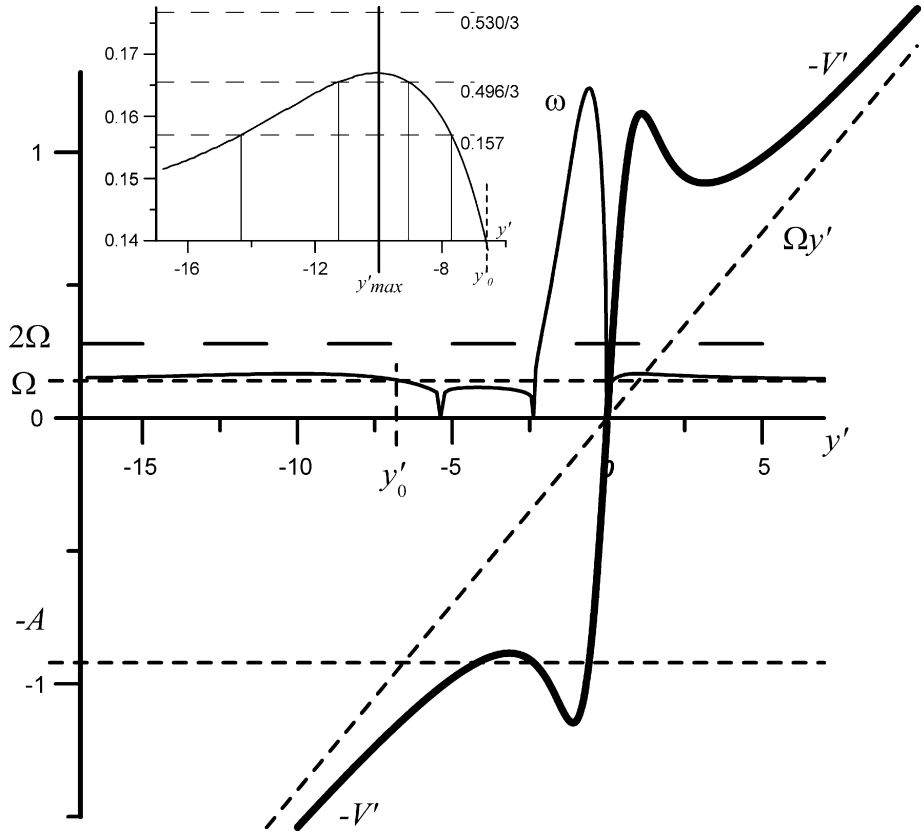

Fig. 1. Profiles of $-V'$—azimuth velocity (6)—heavy line—and the circulation frequency of fluid particles along closed trajectories ω—fine line—as functions of variable y'—at $x' = 0$ in the coordinate system rotating with a constant frequency $\Omega = 0.14$. The inset with extended vertical coordinate shows the behavior of function ω in the vicinity of its maximum. Values of the numerical parameters are explained in the comments to Figs. 8 and 9 (see the text).

[3] Note that the singular points will be stationary only in a rotating coordinate system.

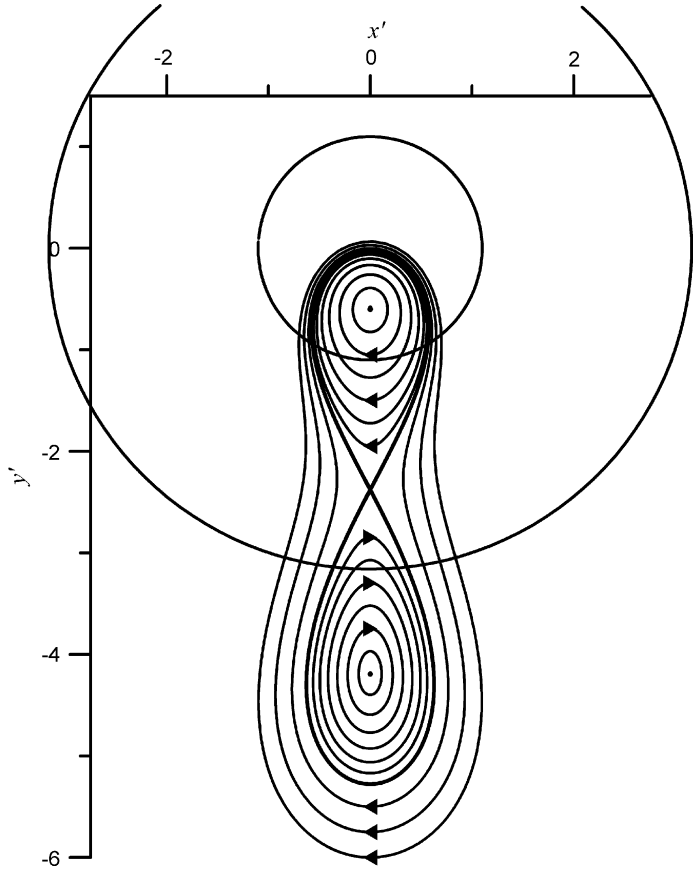

Fig. 2. Isolines of the stream-function Ψ' in the co-rotating frame at $\Omega = 0.14$, $A = B = 0.92$ and $u_0 = v_0 = \mu = \omega_0 = \varphi_0 = 0$ (there are two elliptic and one hyperbolic singular points). The circular curves are the boundaries of neutral stability in a linear approximation (explanations are given in the text). The heavy line is the separatrix separating three domains with qualitatively different flows.

The example with $A = 0.92$ (the lower horizontal dashed line in Fig. 1) illustrates such a situation. In this case, there exist two topographic vortices moving along circular trajectories around a common rotation center. Function ω takes zero values in points lying on the separatrix (including its hyperbolic point) and takes extreme values in the elliptic points of the phase portrait.

The corresponding streamline pattern is given in Fig. 2. Hereafter, the vortices localized in the upper and lower loops of the separatrix will be referred to as inner and outer topographic vortices.

The origination of chaos in non-autonomous systems of the form (8) is closely related to the stability features of the trajectories of individual fluid particles, though these problems are not equivalent (Pierrehumbert and Yang, 1993). The local stability is determined by the eigenvalues of matrix

$$\begin{pmatrix} u_x & u_y \\ v_x & v_y \end{pmatrix},$$

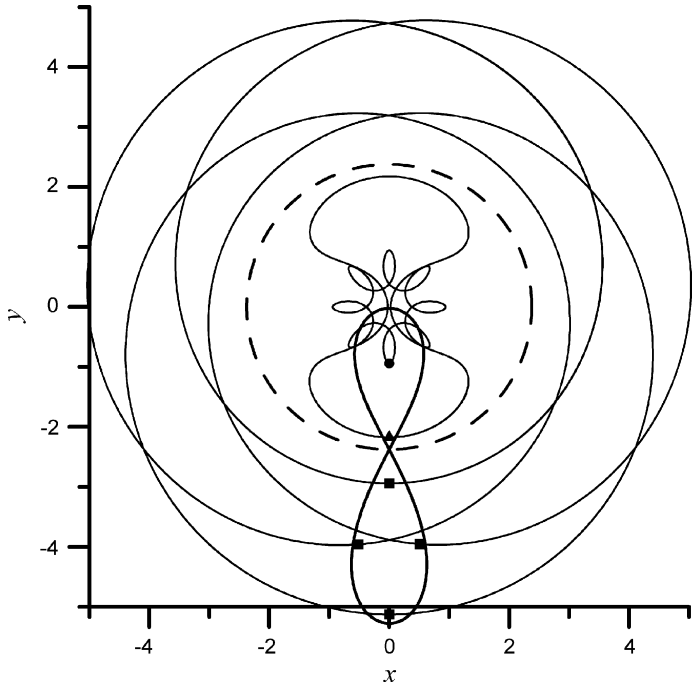

Fig. 3. Examples of periodic trajectories for the same parameters as in Fig. 2 and $v = 8$, 2 for particles from the inner vortex (two trajectories) and $v = \frac{3}{4}$ for a particle from the outer vortex. Markers show the position of the chosen fluid particle after one period: the circle (one) is for the first curve, the triangle (one) is for the second curve, and the squares (four) are for the third curve (the initial point in it occupies the position closest to the center, while the other points alternate cyclically in the anticyclonic direction). The dashed circumference denotes the trajectory of the hyperbolic point of the separatrix.

satisfying the equation $\lambda^2 = \Delta \equiv v_x u_y - u_x v_y$. Calculations, similar to those carried out in Izrailsky et al. (2004), yield the expression

$$\Delta' = -\frac{1}{2r}\frac{\mathrm{d}V'^2}{\mathrm{d}r}. \tag{9}$$

Clearly, the states within the circle $r < r_1$ and outside the circle $r > r_2$ (r_1 is the position of the minimum of azimuth velocity, r_2 is the position of its maximum) are stable in the linear approximation, while the states in the ring $r_1 < r < r_2$—are unstable (see Fig. 2). The domain of linear instability commonly features chaotization in the vicinity of the separatrix (Kozlov and Koshel, 1999); however, as will be seen below, the trajectories that never come into the instability domain can also have chaotic properties.

When the ratio of the frequency of fluid particle circulation to the frequency of variations in the external flow $v = \omega(r)/\Omega$ is rational, the trajectories of fluid particles are closed and periodical, and hence, theoretically, a denumerable set of periodic solutions can exist.

The motions of fluid particles (even those involved in periodic motions) in the fixed system of coordinates can have complex structure (see Fig. 3, where the initial position of the separatrix is shown for the comparison of the spatial scales).

At the given set of the external parameters, the maximum frequency of the cycle $\max \omega(r) = \omega_{\max} = 1.2412$ is attained in the vicinity of the elliptic point that is closest to the center (Fig. 1), and, thus, $[v_{\max}] = [\omega_{\max}/\Omega] = 8$ where the square brackets denote the integral part of the respective expression.

Fig. 3 gives examples of periodic trajectories for the cases of $v = 8$, 2 and $\frac{3}{4}$. It is clear (and confirmed by Fig. 3), that when parameter v is an integer, the particle that was on the y-axis at $t = 0$, will return to the initial position within each cycle, and at $v = \frac{3}{4}$ will return in this position only after four periods (that is why the corresponding Poincaré cross-sections for the first two variants contain one point each, and those for the third variant contain four points).

Numerical simulations show that the outer topographic vortex does not contain trajectories with a whole v, while in the domain outside of the vortex, the resonance conditions are satisfied only at $v = 1$ (this is not shown in the figure).

3. Disturbed system

If at least one of the perturbations is nonzero, the stream-function, according to (7), becomes unsteady and chaotic trajectories can appear. This, on the one hand, resembles the situation discussed in Izrailsky et al. (2004), where weak perturbations may cause the formation of a chaotic layer in the vicinity of the separatrix, and, on the other hand, the rotation center can be regarded as an elliptic point of a hypothetic phase portrait with a hyperbolic point at infinity. This determines the origination of noninear resonances in the outer domain and in the chaotic domains associated with them (Zaslavsky, 2007; Chirikov, 1979; Koshel and Stepanov, 2006a). The nonlinear resonances appear in the form of vortices-satellites (or stability islands) rotating around a system of vortices trapped by the topography. Thus, two opposite trends can be seen: first, the chaotization of trajectories causes active mixing of fluid particles, and, second, nonlinear resonances facilitate the formation of ordered (coherent) structures.

3.1. Effect of the unsteady character of the external flow perturbation

The distribution of the circulation frequency of fluid particles (Fig. 1), as a function of the distance between the initial position of the trajectory and the rotation center, shows that its derivative within the inner topographic vortex is relatively large, and hence, in accordance with the Chirikov criterion (Chirikov, 1979; Zaslavsky, 2007; Koshel and Stepanov, 2006a), the width of a domain of possible nonlinear resonances should be narrow. By contrast, the derivative of function ω should be small for the outer topographic vortex and in the domain beyond the vortex, while the widths of the resonance[4] should be wide.

This is confirmed by Fig. 4a, which shows Poincaré cross-section for a small-amplitude unsteady perturbation of the velocity modulus of the external flow ($\mu = 0.02$) with a frequency of $\omega_0 = \Omega = 0.14$. Note that hereafter we will construct Poincaré cross-sections in a rotating coordinate system, determining the positions of marker particles with a period of $T = 2\pi/\kappa$, where $\kappa = \omega_0$, if $\mu \neq 0$ and $\kappa = \Omega$ or $\kappa = 2\Omega$, if $\mu = 0$.

Indeed, the chaotization layer in the outer topographic vortex is much wider than in the inner layer, and we have a zone of nonlinear resonance, surrounded by a wide stochastic layer, beyond the separatrix. The latter, in its turn, is surrounded by a chain of nonlinear resonances with a fairly high multiplicity.[5]

[4] Hereafter, *the width of the domain of the nonlinear resonance* will be used to denote the interval between the maximum and minimum frequencies of the trajectories that fill this domain.

[5] We will not study the fractal structure of the phase space, since it has been quite well studied (Budyansky et al., 2002, 2004a, b; Zaslavsky, 2007). The manifestations of fractality are typical in our model.

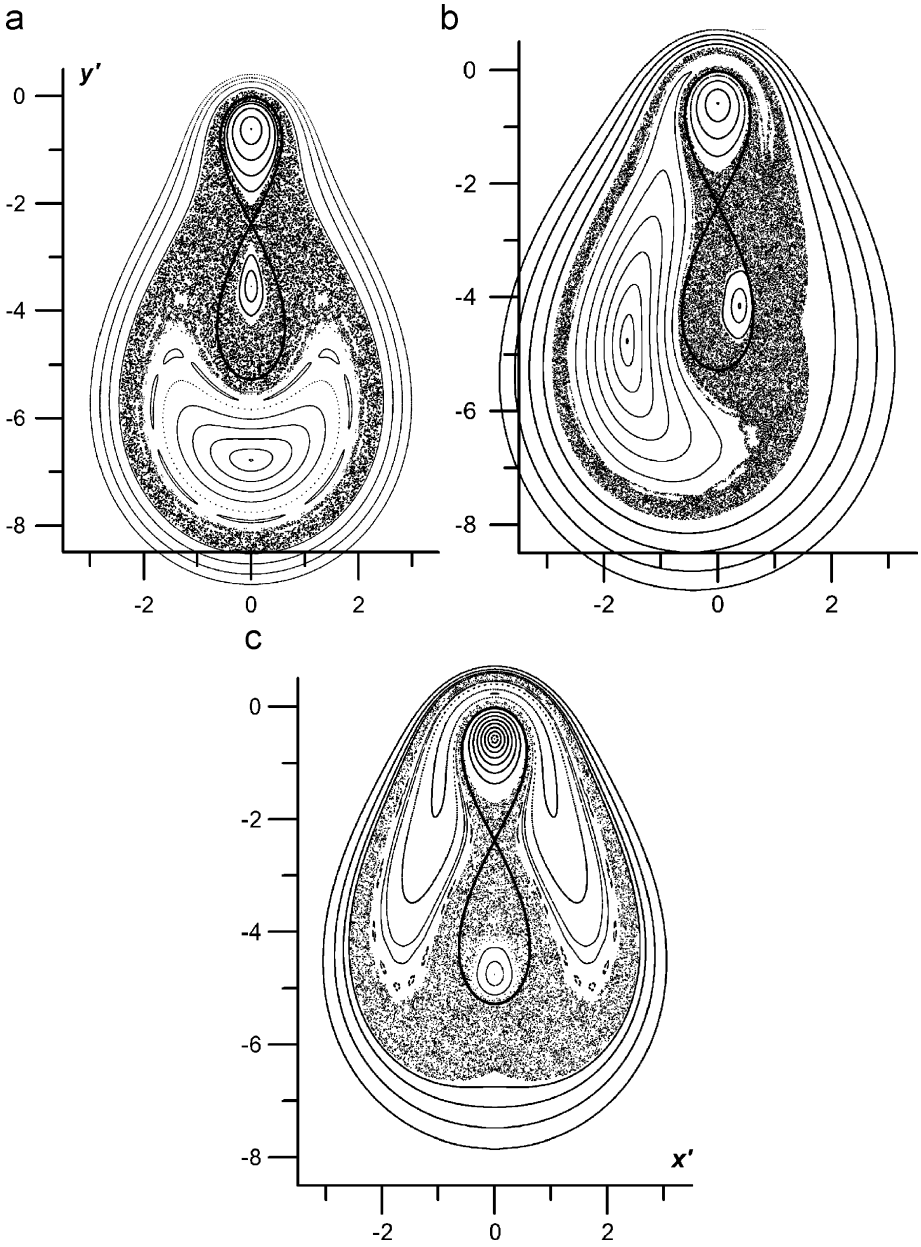

Fig. 4. Poincaré cross-sections at $\Omega = 0.14$, $A = B = 0.92$, $u_0 = v_0 = 0$, $\mu = 0.02$, $\omega_0 = 0.14$ for the cases: (a) $\varphi_0 = 0$, (b) $\varphi_0 = \pi/2$, (c) $\varphi_0 = \pi$. The separatrix of the undisturbed motion is shown here and in the following figures by a heavy line.

At $\varphi_0 = 0$, the domain of external nonlinear resonance in Fig. 4a forms in the vicinity of the trajectory[6] with the rotation frequency $\omega(y_0') = \kappa = \omega_0$ (point y_0' is marked in Fig. 1 by a dashed vertical segment).

Following Zaslavsky (2007), we will say that the nonlinear resonance established in a trajectory with the rotation frequency of $\omega(y') = (m/n)\kappa$, has *a rotation number* of m/n. The whole variable n, equal to the number of islands (elliptic and hyperbolic points) will be referred to as *resonance multiplicity*,

[6] The term *trajectory* is used here in the meaning of Poincaré cross-section.

and m, i.e., the number of periods during which the trajectory travels over all islands, will be called the *resonance order*. The nonlinear resonance mentioned above has the rotation number of $\frac{1}{1}$.

The position of elliptic and hyperbolic points of nonlinear resonance is determined by the perturbation phase. As can be seen from Figs. 4b and c, when $\varphi_0 \neq 0$, the domain of this nonlinear resonance still overlaps smaller resonances and partially decomposes; the place it occupies in the periphery of the chaotic sea is determined by the phase of the periodic perturbation of the flow. The change in the perturbation phase has a slight effect on the position of the outer topographic vortex.

The comparison of Figs. 4a and 5a allows us to elucidate the role of μ—the amplitude of unsteady perturbation: with increasing μ, the chaoticity domain increases, the regular part of the inner vortex declines, advecting particles almost completely fill the zone of outer topographic vortex, and the domain of the main nonlinear resonance also decreases. This can be explained by an increase in the width and the extent of overlapping of all nonlinear resonances.

Doubling of the frequency of an unsteady perturbation (Fig. 5b) results in a situation with less degree of chaotization in the zones of inner and outer topographic vortices, and a resonance, comprising two vortices, forms in the outer domain instead of the nonlinear resonance $\frac{1}{1}$. Really, there are no trajectories with the rotation frequency of 2Ω, and the condition for the formation of the first large nonlinear resonance comprising two vortex domains is fulfilled now on a trajectory with the rotation frequency equal to half the perturbation frequency (the rotation number of $\frac{1}{2}$). The latter agrees well with Fig. 1, according to which, at the frequency of $\omega_0 = 2\Omega$, there is no trajectory with the appropriate rotation frequency below the outer vortex, while the curves cross at the frequency of $\omega(y'_0) = \omega_0/2 = \Omega$.

Note also that, as follows from formula (7), doubling of the perturbation frequency is equivalent to a small elliptic perturbation of a circular external flow with $\mu = 0$ and $A > B$. Fig. 5c (where $A/B \approx 1.069$) is a confirmation of this effect, showing a virtually analogous structure of Poincaré cross-section.

Until now we have considered the perturbation frequencies that are multiple to the rotation frequency of the external flow Ω. Let us pass to the more interesting case of arbitrary ω_0.

Analysis of Fig. 1 can be of great use for the interpretation of Poincaré cross-sections, since it allows one to predict the main features of the phase portrait of a disturbed system. In this case, we follow the assumption, which was numerically confirmed by Izrailsky et al. (2006), that the conclusions about the position and width of nonlinear resonance domains that were drawn from the analysis of undisturbed frequency $\omega(y')$ are still valid for nonzero and even sufficiently large perturbations μ.

Let us consider, for example, horizontal line $\omega_0 = 0.157$ (see the inset in Fig. 1). This line crosses (in the outer domain) the curve $\omega(y')$ in two points—close to the center and further from the center—on the opposite sides of the vertical line $y'_{\max} = -9.9913$ such that $\omega(y'_{\max}) \equiv \omega_{\max} = 0.16699$. At the frequency under consideration, at least for small perturbations μ, two nonlinear resonances with rotation numbers of $\frac{1}{1}$ should be expected to appear. The critical points of the resonance domains should be located at the y'-axis in the points determined by the appropriate vertical lines in the inset in Fig. 1. Indeed, these conditions are satisfied with a great accuracy for the coordinates of the hyperbolic point of external resonance and the elliptic point of the internal resonance in Fig. 6a, where $\mu = 0.02$.

It is clear that, as the perturbation frequency increases, while $\omega_0 < \omega_{\max}$, the external and internal nonlinear resonances will move closer to one another. It is reasonable to expect that, at some frequency (sufficiently close to the maximum frequency of rotation), the separatrices will reconnect (Howard and Hohs, 1984; del-Castillo-Negrete and Morrison, 1993). A manifestation of this effect is shown in Figs. 6 and 7. These figures show a thin chaotic layer in the vicinity of some separatrices; however, one can easily imagine the situation that will form at weaker perturbations. At the perturbation frequency of $\omega_0 = 0.157$,

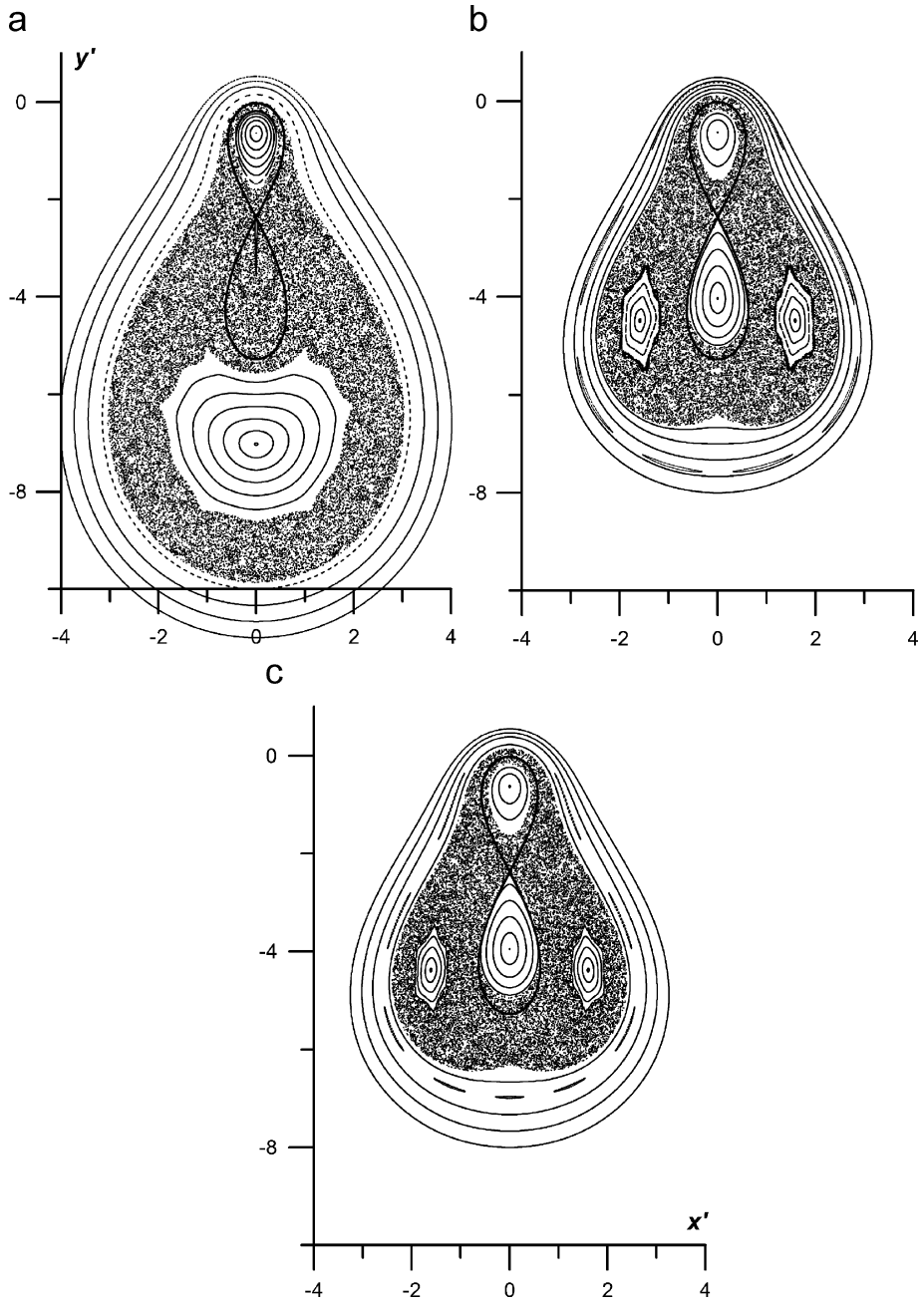

Fig. 5. Poincaré cross-section at $\Omega = 0.14$, $u_0 = v_0 = 0$, $\varphi_0 = 0$ for the cases: (a) $A = B = 0.92$, $\mu = 0.05$, $\omega_0 = 0.14$; (b) $A = B = 0.92$, $\mu = 0.05$, $\omega_0 = 0.28$; (c) $A = 0.92 \cdot 1.034$, $B = 0.92/1.034$, $\mu = 0$, $\omega_0 = 0$.

we see a separatrix, which is quite common for nonlinear resonances and can be regarded as heteroclinic (a more vivid case for resonances $\frac{1}{3}$ will be shown below). Note that an appreciable stochastic layer can be seen only in the vicinity of the internal separatrix. The situation radically changes at $\omega_0 = 0.163$. At this frequency, we see two homoclinic structures, where the separatrices have changed places, and the branches of the initially internal separatrix now embrace the second nonlinear resonance, the branches of

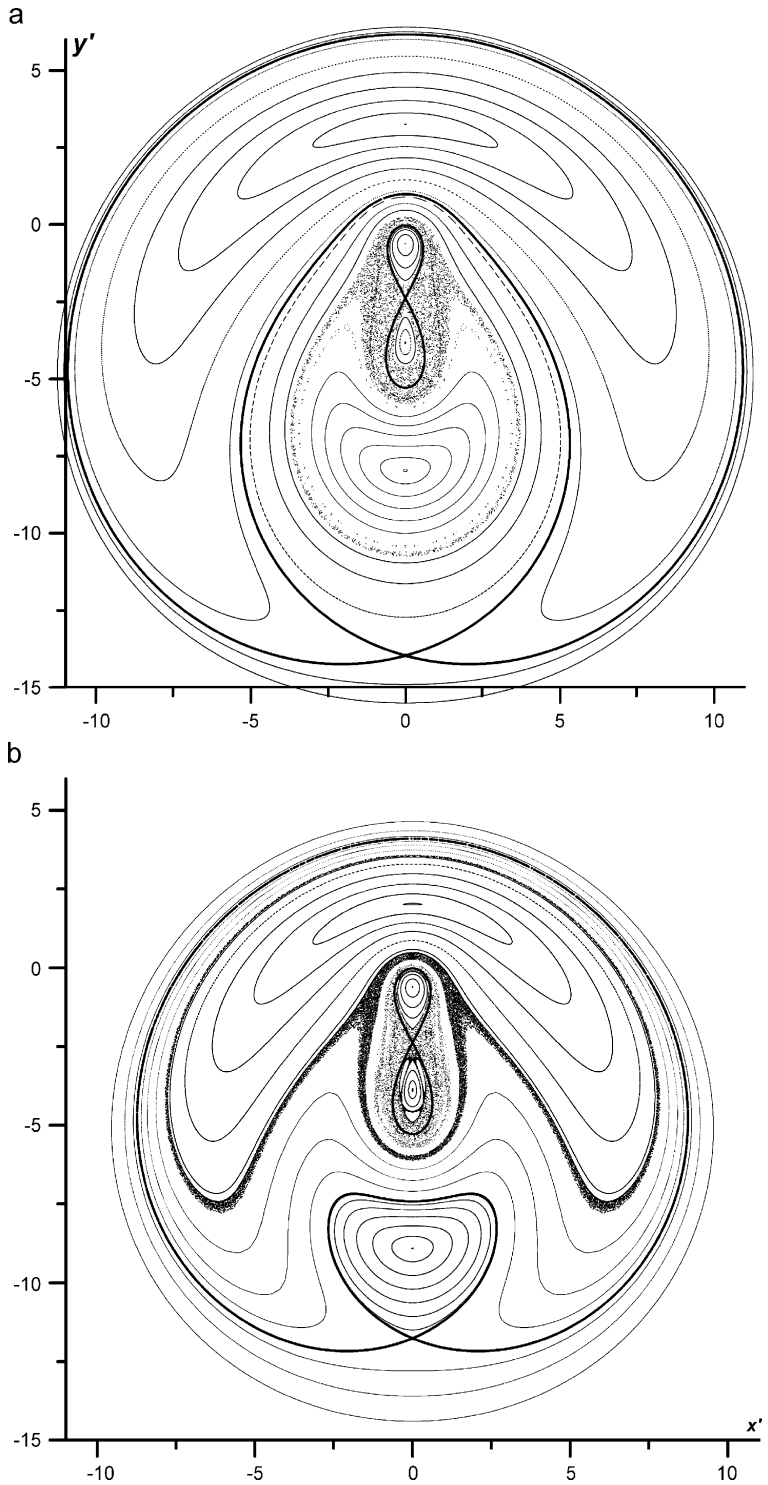

Fig. 6. Poincaré cross-sections at $\Omega = 0.14$, $A = B = 0.92$, $u_0 = v_0$, $\mu = 0.02$, $\varphi_0 = 0$ for the cases: (a) $\omega_0 = 0.157$, (b) $\omega_0 = 0.163$.

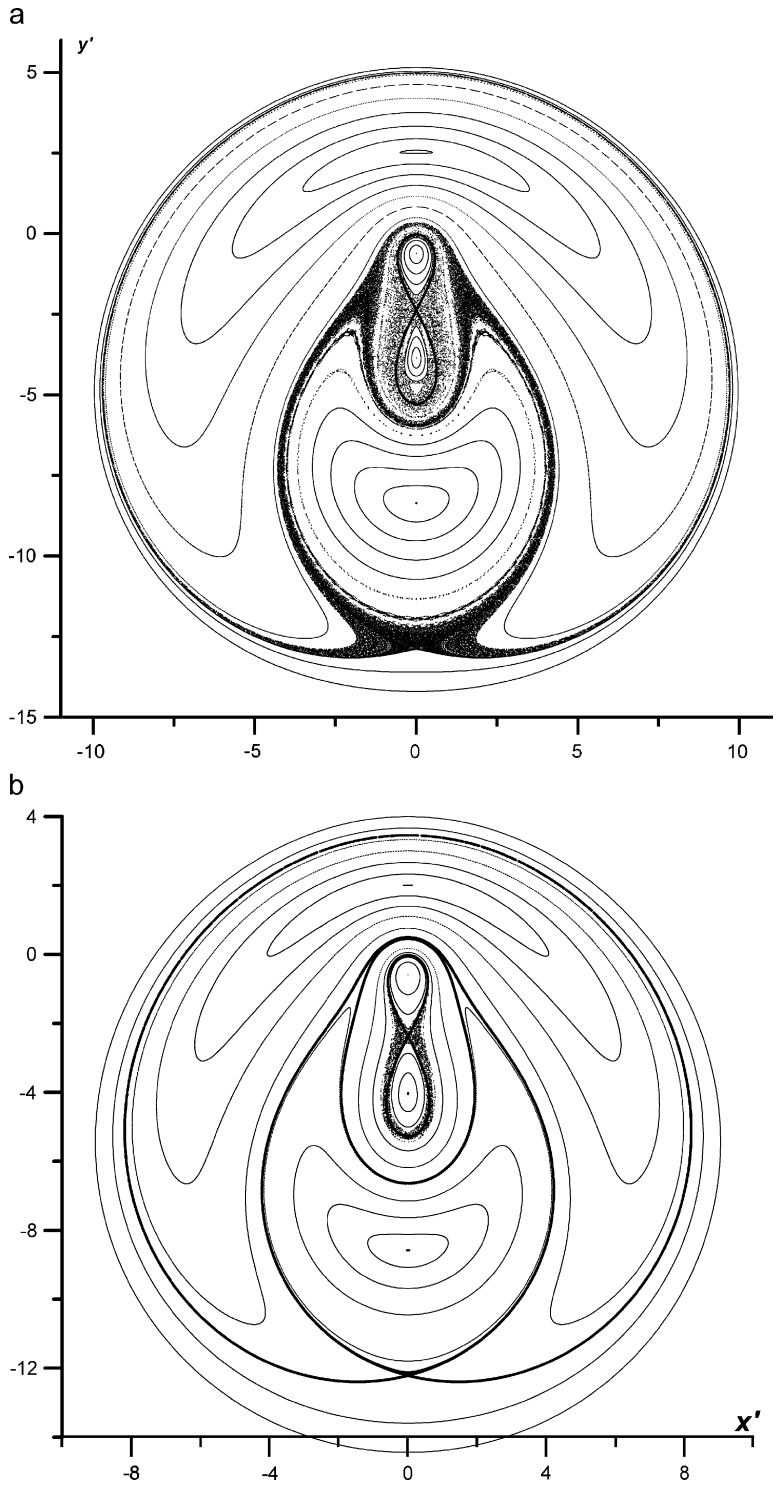

Fig. 7. Poincaré cross-sections at $\Omega = 0.14$, $A = B = 0.92$, $u_0 = v_0 = \varphi_0 = 0$ for the cases: (a) $\mu = 0.02$, $\omega_0 = 0.1601$, (b) $\mu = 0.01$, $\omega_0 = 0.16253$.

whose separatrix now embrace the central domain. It is interesting that before the reconnect, both singular points of each nonlinear resonance were on the same side of the trajectory, corresponding to the maximum rotation frequency of the undisturbed system. Now, the elliptic points remain in the same position relative to this curve, while the hyperbolic points change places, and, accordingly, the singular points of each resonance are located on different sides of the maximum of rotation frequency (see also the inset to Fig. 1). In these two cases, both before and after the reconnect, there exists a barrier consisting of closed trajectories between nonlinear resonances, and the separatrix chaotic layer is sufficiently clear at the separatrix that leads to the internal hyperbolic point. Numerical calculations show that at $\mu = 0.01$, the frequency $\omega_0 = 0.16253$ corresponds to a so-called *global bifurcation* (del-Castillo-Negrete and Morrison, 1993), and the frequency $\omega_0 = 0.1601$ corresponds to a global bifurcation at $\mu = 0.02$, see Fig. 7. In this case we see a merged separatrix and the maximum width of the stochastic layer at $\mu = 0.02$. Thus, a transport passage can form in the vicinity of the global bifurcation frequency, which, as was the case in del-Castillo-Negrete and Morrison (1993), depends on the amplitude of perturbation. Markers can move through this passage from the central domain to the periphery and vice versa. Such passage can form only in the vicinity of the global bifurcation frequency. Zaslavsky (2007) called the effect considered above *weak chaos*. If we increase the amplitude of perturbation at fixed frequency or change the frequency at fixed amplitude, the passage will disappear. Comparison of Figs. 7a and b illustrates the following dependence: the frequency of global bifurcation decreases with increasing perturbation amplitude. This phenomenon allows a simple explanation. Indeed, an increase in the perturbation amplitude is accompanied by an increase in the width of the nonlinear resonance domain (Zaslavsky, 2007), with the result that the condition of tangency for separatrices is violated. The second cause of the absence of the transport passage far from the bifurcation domain is the fact that small perturbations contribute most to the destruction of the separatrix whose hyperbolic point is sufficiently close to the central domain, i.e., to the domain of strong nonlinearity (see Fig. 1).

Thus, a sufficiently good transport passage can exist only at the parameters corresponding to a global bifurcation. However, the motion of markers from the central domain to the periphery is also possible at sufficiently large amplitude, when the roles of internal and external nonlinear resonances interchange after the reconnect: the *new* internal resonance is being destroyed, while the *new* external resonance is being displaced to the periphery. Global chaos forms in this situation. In the case of resonances of the type $\frac{1}{1}$, the width of resonances can be evaluated based on the frequency by using the so-called "pendulum approximations" method (Zaslavsky, 2007; del-Castillo-Negrete and Morrison, 1993). However, this method is inapplicable in the case of resonances with smaller rotation number, since, unlike del-Castillo-Negrete and Morrison (1993), the change to action angle variables in our model is fairly complicated.

Let us consider the frequencies ω_0 that exceed $\Omega \cdot n = 0.14 \cdot n$ for $n = 2,3$. Clearly the system will not contain resonances of the type of $\frac{1}{1}$ in this case, since the condition $\omega_0 > \omega_{\max}$ is valid. However, the line ω_0/n can cross the curve $\omega(y')$ in the external domain on both the left and the right from the maximum. This means that nonlinear resonances comprising n islands will appear at appropriate distances from the center. With an increase in frequency ω_0 the centers of these resonances will approach $y'_{\max}$ and the domains themselves will first increase and next decrease and, finally, they will disappear at $\omega/n = \omega_{\max} + \Delta\omega$. Here $\Delta\omega$ is the width of the domain of the appropriate resonance (Zaslavsky, 2007).

Since the features of the phase portrait at different $n > 1$ are qualitatively similar, we consider in detail the case $\omega_0 \geqslant 3\Omega$ where $(n = 3)$. The corresponding situation with two groups, each comprising 3 stability islands, is presented in Fig. 8. In general, the scenario is analogous to the case of frequencies close to Ω.

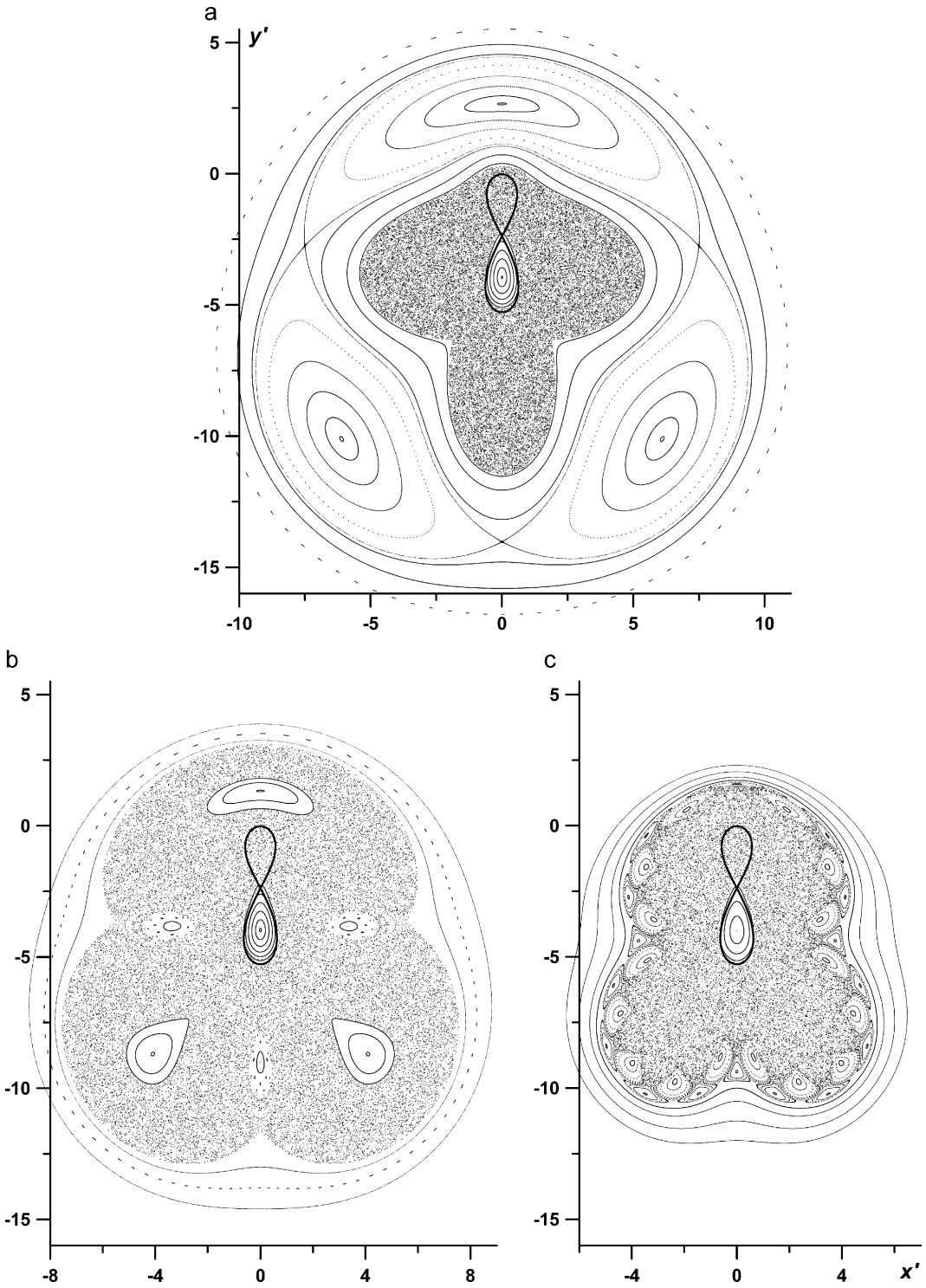

Fig. 8. Poincaré cross-section at $\Omega = 0.14$, $A = B = 0.92$, $u_0 = v_0 = 0$, $\mu = 0.3$, $\varphi_0 = 0$ for the cases: (a) $\omega_0 = 0.475$, (b) $\omega_0 = 0.496$, (c) $\omega_0 = 0.530$.

Thus, in Fig. 8a, the external nonlinear resonance $\frac{1}{3}$, consisting of three vortices, started approaching the internal domain of chaotization, the shape of which is determined by the completely destroyed internal nonlinear resonance $\frac{1}{3}$. However, the external resonance has not been destroyed, since it has not started overlapping with the internal one.

The frequency is higher in Fig. 8b. In this case, the coordinates of the centers of both nonlinear resonance domains are close to the trajectory with the maximum rotation frequency. They are decreasing already, though the area of the chaotization domain is close to the maximum for the case of resonances containing three vortices. This situation illustrates the global chaos that commonly forms at sufficiently large perturbation amplitudes. The figure also shows a reconnect of separatrices—all three vortices of the internal resonance clearly have homoclinic structure. Looking ahead, we note that the decrease in the specified unsteady perturbations by an order of magnitude (Fig. 9) shows that a heteroclinic structure with common hyperbolic points will form at lower frequencies.

In Fig. 8c, where $\omega_0/3 > \omega_{\max}$ (see the appropriate line $0.530/3$ in the inset to Fig. 1), the absence of large nonlinear resonances causes a decrease in the chaotization domain. A similar result was obtained in Izrailsky et al. (2006), where the disappearance of large nonlinear resonances was also accompanied by a decrease in the degree of chaotization of the vortex domain. In the absence of large nonlinear resonances, resonances with large multiplicity and orders emerged. In this case, the boundary of the chaotization domain passes virtually along the trajectory with the frequency $\omega_{\max}$, around which two chains containing 16 vortices (islands of regular behavior) can be seen. The number of periods for these nonlinear resonances can be readily evaluated. Since $\omega(y') < \omega_{\max}$, then, at $\omega_{\max} = 0.16699$ we have $m = [16\omega_{\max}/\omega_0] = [5.04] = 5$.

Thus, we have two domains of nonlinear resonances with rotation numbers of $\frac{5}{16}$. One of these is located closer to the center, and the second is further from it, but both are localized in the vicinity of the trajectory with the frequency of $\omega_{\max}$. Since the relationship $\frac{5}{16}$ is close to $\frac{1}{3}$, the shape of the chaotic domain resembles a trefoil.

Fig. 9 shows Poincaré cross-sections for a sufficiently small perturbation $\mu = 0.03$, which, on the one hand, provides an appreciable width of nonlinear resonances with a rotation number of $\frac{1}{3}$, and, on the other hand, still does not cause significant destruction of their separatrices (neither because of secondary nonlinear resonances, nor because of overlapping of major resonances). This example is convenient for the analysis of the reconnect of separatrices for the case of $n = 3$.

In Fig. 9a the value of ω_0 is lower than the frequency of global bifurcation, i.e., the distances from the resonance domain centers to the maximum-frequency trajectory is greater than the width of these resonances. As mentioned above, both the internal and external vortex chains have a heteroclinic structure. These structures are separated by a domain of closed curves surrounding the rotation center. At this amplitude, the frequency $\omega_0 = 0.496198$ (Fig. 9b) corresponds to the frequency of the global bifurcation. Here the distance between the centers of the domains of nonlinear resonances and trajectories with maximum rotation frequency is equal to their width; hence the separatrices are tangent and merge to form a single trajectory. At each value of the perturbation amplitude, the corresponding frequency of the global bifurcation is optimal for the transportation of particles from the internal into the external domain, since in this limiting case, there is no barrier between the domains of the internal and external resonances, a situation that creates conditions for the overlapping at an arbitrarily small deviation from this value of the perturbation amplitude.

In the following figure, ω_0 exceeds the global bifurcation frequency, and we see the formation of homoclinic structures, where the separatrix of the internal (external) resonance becomes the external

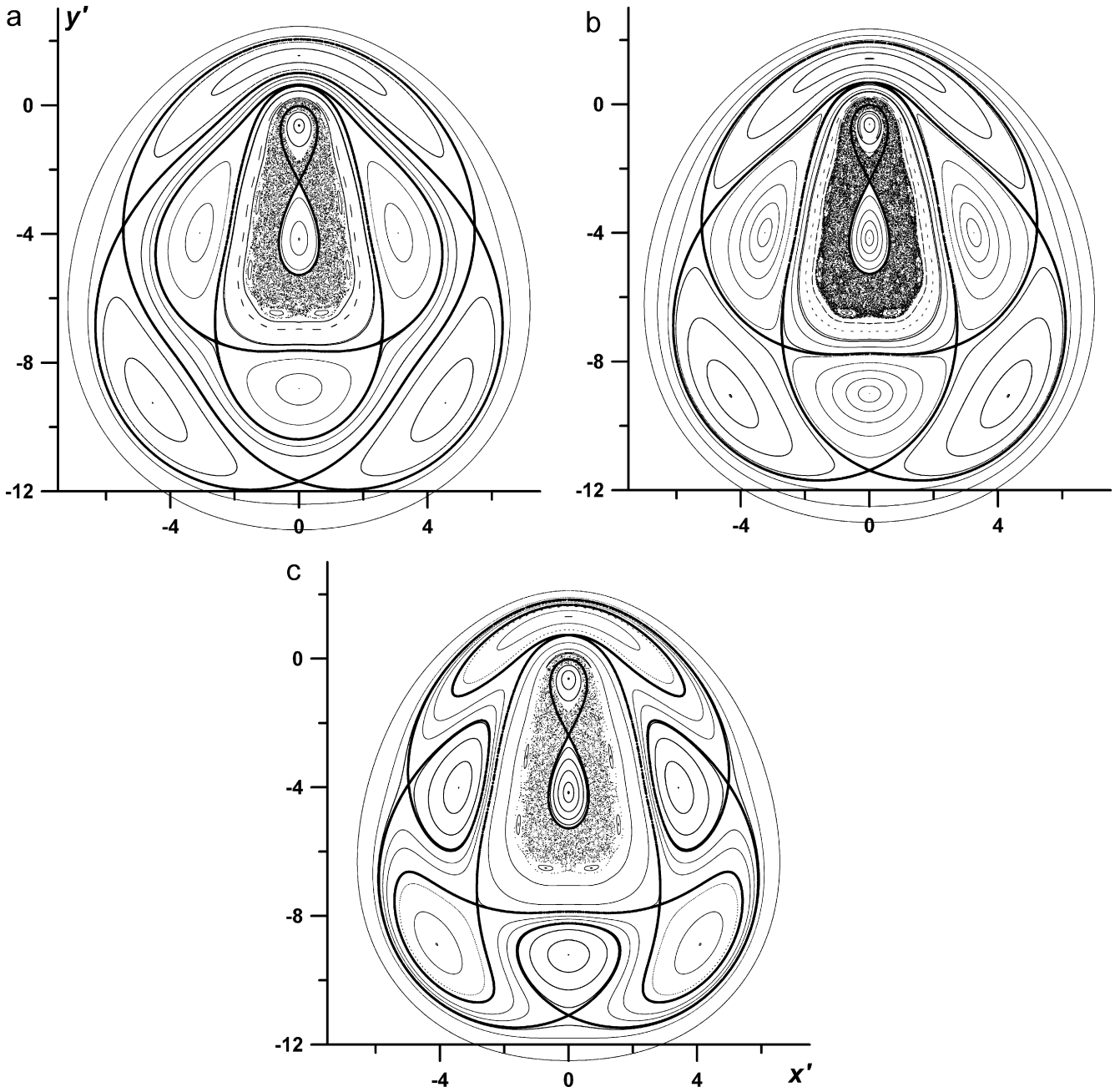

Fig. 9. Poincaré cross-section at $\Omega = 0.14$, $A = B = 0.92$, $u_0 = v_0 = 0$, $\mu = 0.03$, $\varphi_0 = 0$ for the cases: (a) $\omega_0 = 0.494$, (b) $\omega_0 = 0.496198$, (c) $\omega_0 = 0.498$.

(internal) one. The role of the central domain can be distinctly seen here: the two lower vortices of the external resonance have quite standard homoclinic structure, and the upper one is very close to the internal domain, thus creating additional conditions for effective chaotization in the vicinity of its hyperbolic point. Comparing Figs. 9a and c, one can see that, in the bifurcation point, the transformation of both the topological structure of the flow and the configuration of the kinematic barrier in the form of a regular flow takes place.

Note that the chaotic behavior in the vicinity of topographic vortices has qualitative analogues:

- in the problem of the meandering jet stream (del-Castillo-Negrete and Morrison, 1993; Meyers, 1994; Pratt et al., 1995; Lozier et al., 1997; Yuan et al., 2002; Raynal and Wiggins, 2006);
- in the problem of Stokes flow between two cylindrical surfaces (Aref and Balachandar, 1986; Chaiken et al., 1987; Solomon et al., 1994; Meleshko and Aref, 1996; Vainshtein et al., 1996);
- in the problem of three and four discrete vortices (Boffetta et al., 1996; Kuznetsov and Zaslavsky, 1998, 2000; Leoncini et al., 2000, 2001).

We see that the vicinity of the undisturbed trajectory $\omega_{\max}$ plays the same role for the external domain as the elliptic point in the problem of a unidirectional flow (Izrailsky et al., 2006). As the perturbation frequency increases, the nonlinear resonance domains shift toward this trajectory, and after reaching it, they disappear from the system. The general conclusion can be reached that, when perturbations are sufficiently large (global chaos), the maxima of the area of the chaotization domain are attained at frequencies (for the nonlinear resonances of the main series[7]) that are somewhat lower than the maximum rotation frequency $\omega_0 \sim \omega_{\max}/n$. The problem of searching for the perturbation frequency that is optimal for chaotization was posed by Rom-Kedar and Poje (1999). An efficient method for determining the optimal frequencies was proposed by Izrailsky et al. (2006). This method is applicable to this model as well.

The maximum area of the chaos domain here is either equal to the area encompassed by the undisturbed trajectory with maximum rotation frequency, or exceeds it by no more than the width of the nonlinear resonance of the main series (see Fig. 8). Asymptotic estimates and numerical calculations show that, with increasing m and n, the width of the nonlinear resonance domain declines faster than $\mu^{1/2}/mn$.

3.2. *The effect of ellipticity of the external flow*

As was mentioned in the discussion of Figs. 5b and c, the effect of weak ellipticity of the external flow manifests itself as a nonlinear resonance of the form $\frac{1}{2}$, which consists of two vortex domains of regular motion in the periphery of the external topographic vortex. A simple explanation was also given there for this result through the use of an evident analogy between the ellipses specified by the values of their semi-axes A and B[8] and the ellipses that form because of an unsteady perturbation of an axisymmetrical flow with a frequency of $\omega_0 = 2\Omega$ in (1). An insignificant increase in the eccentricity of the ellipse (or perturbation amplitude) results in the formation of a chain of small vortices (nonlinear resonances) within and on the boundary of the mixing layer that formed instead of the undisturbed separatrix.

As the eccentricity of the ellipse increases, nonlinear resonances are produced by more and more steady trajectories, and the formation of stochastic layers (which later merge) takes place in the vicinity of their separatrices. Thus, we can suppose that the phase portrait will consist of a well mixed core, which may contain small stability islands and may be surrounded by chains of vortices—satellites that form instead of steady trajectories.

Poincaré cross-sections for the cases $A/B = 1.69$ and $A/B = 2.25$ are given in Figs. 10a and b, respectively. It can be seen that only one external topographic vortex persisted in the central domain,

[7] The notion of *nonlinear resonances of the main series* will be given in the following section.

[8] In all calculations, we will take $AB = 1$, assuming the conservation of the area of the effective ellipse.

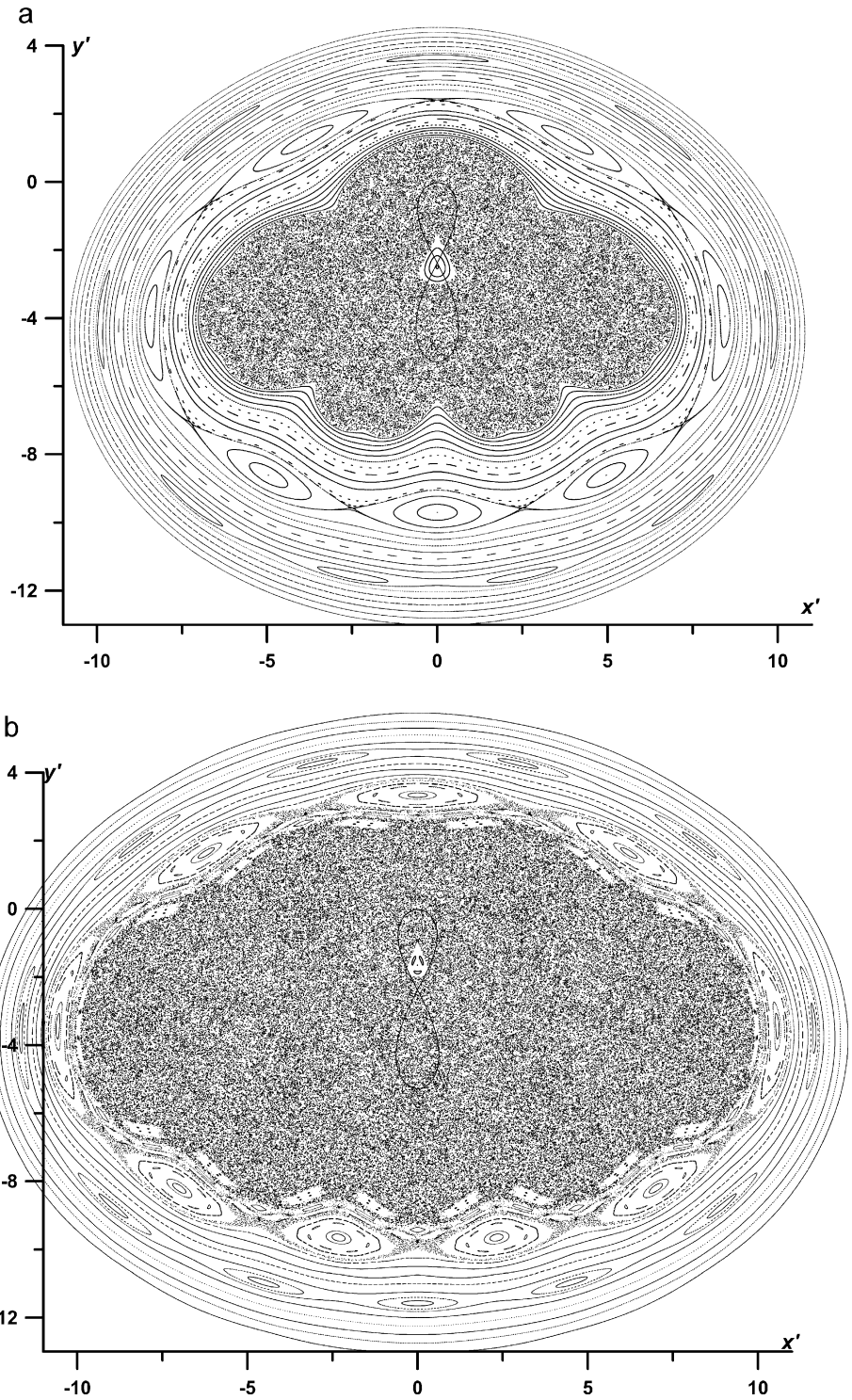

Fig. 10. Poincaré cross-section at $\Omega = 0.14$, $u_0 = v_0 = \mu = \omega_0 = \varphi_0 = 0$ for the cases: (a) $A = 0.92 \cdot 1.3$, $B = 0.92/1.3$; (b) $A = 0.92 \cdot 1.5$, $B = 0.92/1.5$.

while the internal vortex was completely destroyed. Indeed, as was noted above, nonlinear resonances with a multiplicity of 1 and an order from 1 to 8 can theoretically form in the internal vortex. The corresponding domains are fairly wide and, in the case of sufficiently large ellipticity, they overlap. In this case, the trajectories become chaotic in accordance with Chirikov's criterion. The largest resonance in the external vortex has the rotation number of $\frac{1}{2}$, and its width is insufficient to cover the entire vortex domain. The resonance domains of higher orders have even smaller widths.

At $\Omega = 0.14$, when $\omega_{\max} = 0.16699$, the sequence of inequalities can be readily obtained

$$0.595 = \frac{\omega_{\max}}{2\Omega} > \frac{m}{n} = \left[\frac{\omega}{\omega_0}\right] > \frac{\Omega}{2\Omega} = 0.5. \tag{10}$$

Since the analysis of nonlinear resonances is commonly based on the methods of averaging over fast oscillations (Chirikov, 1979; Zaslavsky, 2007), it is clear that the greater the m, the lesser the width of the corresponding nonlinear resonance. Let us introduce the notion of the *main series* of nonlinear resonances. This notion will include the nonlinear resonances from the external domain (outside of the separatrix) for which the rotation number falls within interval (10) for the given n and minimal m. These resonances are the widest, and, overlapping one another, they determine the chaotization of the phase space.

Fig. 10 shows that the width of the resonances that do not belong to the main series is so small, that they are irresolvable at a large distance from the center at our discretization accuracy, while the resonances with large m that fall within interval (10) are sufficiently small to have a significant effect on the overall picture. This accounts for the formation of resonances of the main series $\frac{4}{7}$ and $\frac{5}{9}$ shown in Fig. 10a. The resonances $\frac{2}{5}$, $\frac{1}{3}$ and $\frac{2}{3}$ cannot form. The resonance $\frac{3}{5}$, which forms in the trajectory with the rotation frequency of $0.6 \cdot 2\Omega$ (which is sufficiently close to the boundary value $0.595 \cdot 2\Omega$), goes beyond the limits (10), though it has some effect on the behavior of trajectories—the boundary of the chaotization domain has distinct pentagonal symmetry.

As mentioned above, the width of resonances rapidly declines with increasing n. Thus, we can already characterize the standard chaotization scenario of the external domain, which is realized at all types of perturbations with some deviations that do not affect its general character. The increase in the perturbation amplitude (the eccentricity of the ellipse) is accompanied by the extension of the domain of the last destroyed nonlinear resonance, which determines the external boundary of the zone of chaotic behavior of trajectories. The resonances of the main series, which follow this resonance and correspond to larger n values, also extend and become visible. The largest among them in Fig. 10a are resonances containing 7 and 9 vortices. At the further growth of the perturbation amplitude, the boundary of the irregular-behavior domain overlaps the nearest nonlinear-resonance domain, and now the shape of the boundary of chaotization domain is determined by the order of this resonance.

Thus, Fig. 10b gives the situation preceding the absorption of a resonance consisting of nine islands. The previous resonance consisting of seven islands is already completely destroyed and absorbed by the domain of irregular behavior. The resonance consisting of nine islands has already started the destruction because of overlapping with smaller resonances that do not belong to the main series and secondary resonances that form because of the interaction between the primary ones (Zaslavsky, 2007). However, the domain of the resonance is still isolated from the main chaotic domain by chains of smaller resonances and KAM-tori. The stochastic layer in the vicinity of the separatrix of the 11-vortex nonlinear resonance is too small to resolve.

Note an interesting feature: almost all resonances with even orders are very small and have virtually no effect on the structure of the phase portrait; the only exception is the resonance $\frac{1}{2}$.

Fig. 11a, where $A/B = 2.56$, illustrates the beginning of the process of merging of the resonance $\frac{5}{9}$ with the main domain of irregular behavior. The extended stochastic layer in the vicinity of the separatrix of this resonance has merged with the stochastic sea of the main chaotic-behavior domain; however, the chain of nine vortices has not been destroyed completely. As the perturbation amplitude increases further, the process reiterates with vortex chains of greater multiplicity, so that a chain of 17 vortices is in such situation in Fig. 11b.

This variant can be considered limiting in some sense, since at $A \gg 1$, $AB = \text{const}$, the external flow is in essence an alternating zonal flow (along the y' coordinate). In this case, the transitional character of the flow manifests itself in the appearance of two elongated topographic vortices in the central domain.

3.3. The effect of the irrotational component of the external flow

Taking into account the nonzero values of u_0 and v_0, according to (1), allows one to study the role of the irrotational components of the external flow in the zonal and meridional directions, respectively. However, since all directions in f-plane are equivalent, we can assume that $u_0 \neq 0$, $v_0 = 0$ without loss of generality.

When $A = B = \mu = 0$, the flow in the vicinity of the elevation is regular, and its specific features have been studied well (Huppert and Bryan, 1976; Kozlov and Sokolovskiy, 1980). At $\mu \ll 1$ and "cylindrical" (i.e., depending only on one horizontal coordinate) no chaotization will also exist in the irregularities of the bottom relief (Kozlov and Sokolovskiy, 1980, 1981).

In this section, we will study some features of the effect of the nonsteady irrotational component with the assumption that

$$A = B = v_0 = 0.$$

In this case, the expression for stream-function (1) can be written as

$$\Psi(r, \varphi, t) = \Psi_0(r) + u(t)\Psi_1(r, \varphi, t), \tag{11}$$

where

$$\Psi_0(r) = \int_0^r V(\rho)\,\mathrm{d}\rho, \quad \Psi_1(r, \varphi, t) = -r\sin\varphi, \quad u(t) = u_0[1 + \mu\cos(\omega_0 t + \varphi_0)], \tag{12}$$

and (r, φ) are polar coordinates.

Let us consider the case $u(t)$, $\dot{u}(t) \ll 1$, where, on the one hand, the effect of the topographic trapping is the strongest, and, on the other hand, $u(t)$ can be used as a small parameter for asymptotic analysis.

Unlike the case considered above, we can introduce here the action-angle variables (I, φ), where $I = r^2/2$. Now instead of (11) and (12) we have

$$\Psi(I, \varphi, t) = \Psi_0(r) + u(t)\Psi_1(I, \varphi), \quad \Psi_0(I) = \int_0^{\sqrt{2I}} V(\rho)\,\mathrm{d}\rho, \quad \Psi_1(I, \varphi) = -\sqrt{2I}\sin\varphi. \tag{13}$$

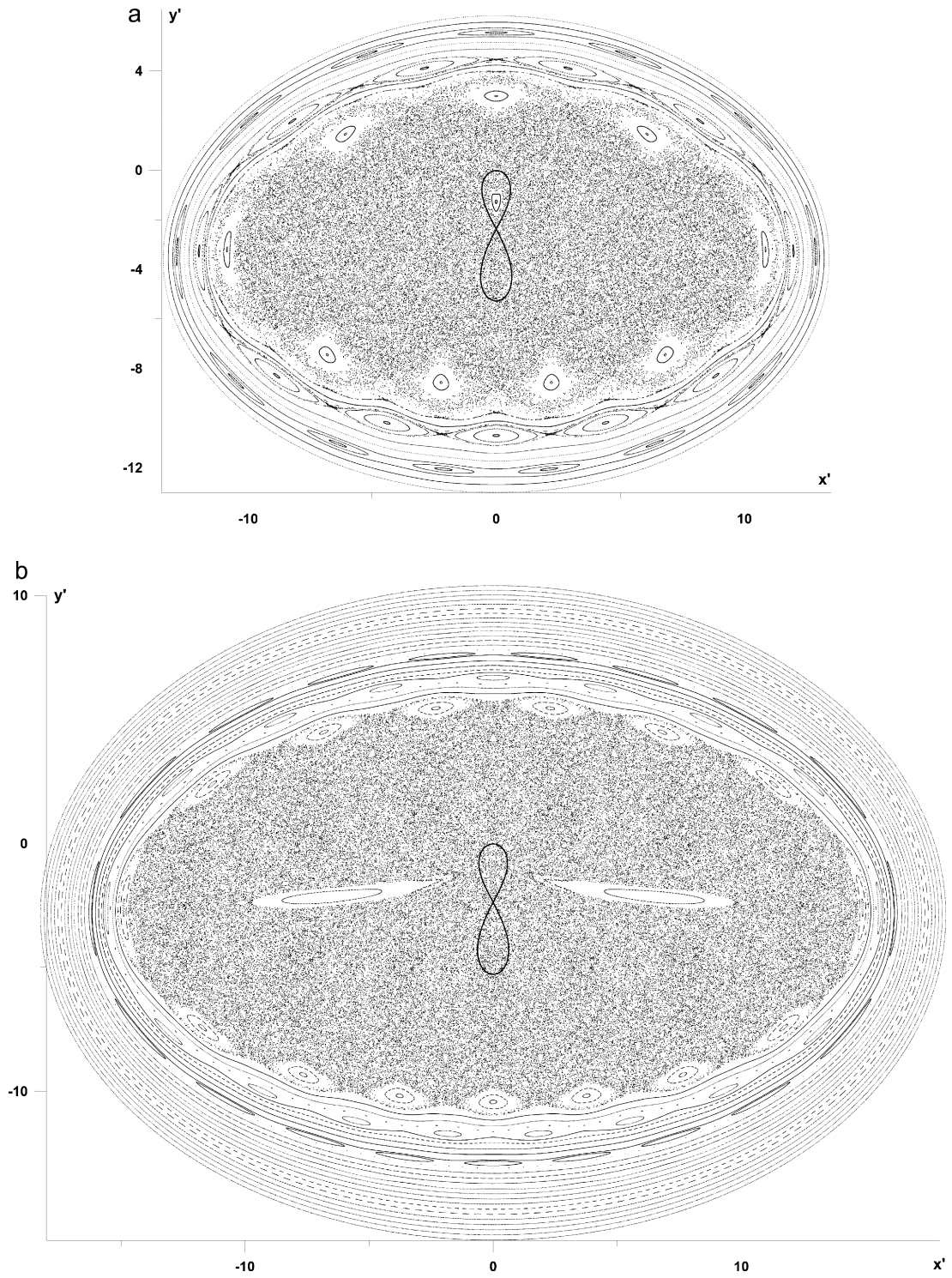

Fig. 11. Poincaré cross-section at $\Omega = 0.14$, $u_0 = v_0 = \mu = \omega_0 = \varphi_0 = 0$ for the cases: (a) $A = 0.92 \cdot 1.6$, $B = 0.92/1.6$; (b) $A = 0.92 \cdot 2$, $B = 0.92/2$.

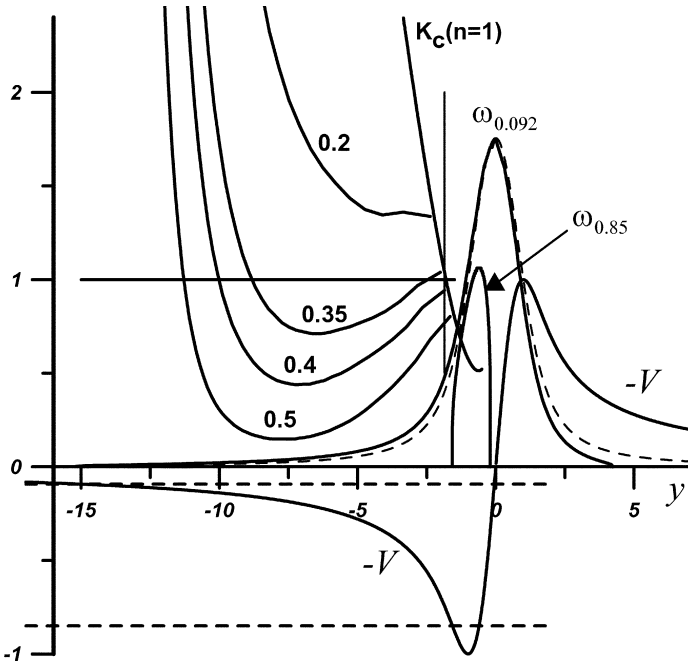

Fig. 12. Profiles of $-V$—azimuth velocity (3) at $A = B = v_0 = 0$ (heavy line) and rotation frequencies of fluid particles along closed trajectories ω (fine line) as functions of variable y at $x = 0$. Two dependencies of rotation frequencies are given: for $u_0 = 0.85$ and $u_0 = 0.092$. The dashed line shows the dependence $\omega(y) = V(y)/y$ for $u_0 = 0.092$. The horizontal dashed lines correspond to values u_0 of 0.85 and 0.092. There are also shown the dependencies $K_c(n, J_n(\omega_0), y)$ for the specified values of perturbation frequencies and $K_c(1, J_1, y)$ for the resonance $\frac{1}{1}$. The full horizontal line shows the critical value 1 of the overlapping criterion.

The equations of motion in a zero approximation take the form

$$\frac{\mathrm{d}I}{\mathrm{d}t} = -\frac{\partial \Psi_0}{\partial \varphi} = 0,$$
$$\frac{\mathrm{d}\varphi}{\mathrm{d}t} = \frac{\partial \Psi_0}{\partial I}, \tag{14}$$

from where we obtain

$$\omega(I) = \frac{V(I)}{\sqrt{2I}}. \tag{15}$$

The dependence (15) adequately approximates the rotation frequency of a fluid particle (found numerically) everywhere except for the vicinity of the separatrix. Both dependencies are given in Fig. 12 by the full and dashed lines, respectively.

Following Lichtenberg and Lieberman (1983), Landau and Lifshits (2004), Zaslavsky (2007), and taking t as a parameter, we introduce new variables (J, ψ) with the use of generating function $S(J, \varphi)$, which as a first approximation has the form

$$S(J, \varphi) = J\varphi + u(t)S_1(J, \varphi) + \cdots . \tag{16}$$

For the new stream-function (Hamiltonian) we have with the same accuracy:

$$\overline{\Psi}(J,\psi) = \overline{\Psi}_0(J) + u(t)\overline{\Psi}_1(J,\psi) + \cdots \tag{17}$$

and

$$\begin{aligned} I &= J + u(t)\frac{\partial S_1(J,\psi)}{\partial \psi} + \cdots, \\ \varphi &= \psi - u(t)\frac{\partial S_1(J,\psi)}{\partial J} + \cdots . \end{aligned} \tag{18}$$

Using (18) and (15), we obtain instead of (17) the following equation:

$$\overline{\Psi}(J,\psi) = \Psi_0(J) + u(t)\left[\omega(J)\frac{\partial S_1(J,\psi)}{\partial \psi} + \Psi_1(J,\psi)\right] + \frac{\mathrm{d}u(t)}{\mathrm{d}t}S_1(J,\psi) + \cdots . \tag{19}$$

The specific form of function $S_1(J,\psi)$ is chosen from the condition of independence of the steady component of the Hamiltonian of ψ:

$$\begin{aligned} &\left\langle u(t)\left[\omega(J)\frac{\partial S_1(J,\psi)}{\partial \psi} + \Psi_1(J,\psi)\right] + \frac{\mathrm{d}u(t)}{\mathrm{d}t}S_1(J,\psi)\right\rangle_t \\ &\quad = u_0\left[\omega(J)\frac{\partial S_1(J,\psi)}{\partial \psi} + \Psi_1(J,\psi)\right] = 0, \end{aligned}$$

where $\langle \ldots \rangle_t$ denotes time averaging. From the latter relationship, we obtain the equation for the generating function:

$$\omega(J)\frac{\partial S_1(J,\psi)}{\partial \psi} = -\Psi_1(J,\psi) = \sqrt{2J}\sin\psi,$$

from where it follows:

$$S_1(J,\psi) = -\frac{\sqrt{2J}}{\omega(J)}\cos\psi. \tag{20}$$

And, thus,

$$\begin{aligned} \overline{\Psi}(J,\psi) &= \Psi_0(J) - \frac{\mathrm{d}u(t)}{\mathrm{d}t}\frac{\sqrt{2J}}{\omega(J)}\cos\psi \\ &= \int_0^{\sqrt{2J}} V(\rho)\,\mathrm{d}\rho + u_0\mu\omega_0\frac{\sqrt{2J}}{\omega(J)}\sin(\omega_0 t + \varphi_0)\cos\psi. \end{aligned} \tag{21}$$

To assess the width of the resonance $\frac{1}{1}$, following Zaslavsky (2007), we write equations of motion in terms of the Hamiltonian (21)

$$\begin{aligned} \dot{J} &= u_0\mu\omega_0\frac{\sqrt{2J}}{2\omega(J)}[\cos(\psi - \omega_0 t - \varphi_0) + \cos(\psi + \omega_0 + \varphi_0)], \\ \dot{\psi} &= \omega(J) + u_0\mu\omega_0\frac{\partial}{\partial J}\left[\frac{\sqrt{2J}}{\omega(J)}\right]\sin(\omega_0 t + \varphi_0)\cos\psi. \end{aligned} \tag{22}$$

Suppose that variable J has a resonance value J_1, then, in the vicinity of this resonance we have

$$|\Delta J| = |J - J_1| \ll 1 \quad \text{and} \quad |\psi - \omega_0 t| \approx |\omega(J_1) - \omega_0| t \ll 1.$$

Omitting the rapidly oscillating term in the first equation and the term of the order of u_0 in the second equation of (22), we obtain as a first approximation with respect to ΔJ

$$\begin{aligned} \dot{J} &= u_0 \mu \omega_0 \frac{\sqrt{2J_1}}{2\omega(J_1)} \cos(\psi - \omega_0 t - \varphi_0), \\ \dot{\psi} &= \omega(J_1) + \frac{\mathrm{d}\omega(J_1)}{\mathrm{d}J} \Delta J. \end{aligned} \tag{23}$$

Since the condition of resonance yields $\omega_0 = \omega(J_1)$, Eq. (23) can be written in the simplified form

$$\begin{aligned} \Delta\dot{J} &= -u_0 \frac{\mu}{2} \sqrt{2J_1} \sin\phi, \\ \dot{\phi} &= \frac{\mathrm{d}\omega(J_1)}{\mathrm{d}J} \Delta J, \end{aligned} \tag{24}$$

where the slow angular variable

$$\phi = \psi - \omega_0 t - \varphi_0 + \frac{\pi}{2}$$

is introduced.

The system of equations (24) correspond to the effective Hamiltonian

$$\widetilde{\Psi} = \frac{1}{2} \frac{\mathrm{d}\omega(J_1)}{\mathrm{d}J} (\Delta J)^2 - u_0 \mu \sqrt{\frac{J_1}{2}} \cos\phi, \tag{25}$$

which describes the dynamics of the system in the vicinity of the resonance $\frac{1}{1}$ in terms of canonically conjugate variables $(\Delta J, \phi)$.

Using the Zaslavsky (2007) method, we obtain from (25) estimates for the width of the resonance over the frequency

$$\Delta\omega(J_1) \sim \sqrt{u_0 \mu \sqrt{\frac{J_1}{2}} \frac{\mathrm{d}\omega(J_1)}{\mathrm{d}J}} \tag{26}$$

and the action

$$\Delta J_1 \sim \sqrt{\frac{u_0 \mu \sqrt{2J_1}}{\mathrm{d}\omega(J_1)/\mathrm{d}J}}. \tag{27}$$

Let us denote the distance between the centers of the resonance domains $\frac{1}{1}$ and $\frac{1}{2}$ by δJ. Expanding the approximate equality

$$\omega(J_1 + \delta J) \approx \frac{\omega_0}{2} \approx \frac{\omega(J_1)}{2},$$

in δJ we obtain the estimate

$$|\delta J| \sim \left| \frac{\omega(J_1)}{2(\mathrm{d}\omega(J_1)/\mathrm{d}J)} \right|. \tag{28}$$

For the analysis of the degree of chaotization of the phase space in the vicinity of the nonlinear resonance $\frac{1}{1}$, it is helpful to introduce the function of ratio of half of its width in terms of action to the distance between the centers of the resonance domains $\frac{1}{1}$ and $\frac{1}{2}$, which will be used as a very rough substitution of Chirikov criterion (Chirikov, 1979):

$$K_c = \frac{\Delta J}{2\delta J} \sim \sqrt{\frac{u_0\mu\sqrt{2J_1}\mathrm{d}\omega(J_1)/\mathrm{d}J}{\omega^2(J_1)}}. \tag{29}$$

To assess the width of the resonance domains with high multiplicities, following Lichtenberg and Lieberman (1983) and expanding $S(J, \psi, t)$, we write

$$\begin{aligned}
\overline{\Psi}_0(J,\psi) &= \Psi_0(J) + \sum_{m,n} \frac{1}{n!}\frac{\partial^n \Psi_0}{\partial J^n}\left[u^m(t)\frac{\partial S_m}{\partial \psi}\right]^n,\\
\overline{\Psi}_1(J,\psi,t) &= \Psi_1(J,\psi) + \sum_{m,n} \frac{1}{n!}\frac{\partial^n \Psi_1}{\partial J^n}\left[u^m(t)\frac{\partial S_m}{\partial \psi}\right]^n.
\end{aligned} \tag{30}$$

Since our prime interest is in the amplitudes of nonlinear resonances with the accuracy to the least order with respect to $u(t)$, we pass, by analogy with the above reasoning, to the system

$$\begin{aligned}
\overline{\Psi}_0(J,\psi) &= \Psi_0(J) + \sum_{n} \frac{1}{n!}\frac{\partial^n \Psi_0}{\partial J^n}\left[u(t)\frac{\partial S_1}{\partial \psi}\right]^n,\\
\overline{\Psi}_1(J,\psi,t) &= \Psi_1(J,\psi).
\end{aligned} \tag{31}$$

Thus, the Hamiltonian

$$\overline{\Psi}(J,\psi,t) = \Psi_0(J) + u(t)\Psi_1(J,\psi) + \sum_{n} \frac{1}{n!}\frac{\partial^n \Psi_0}{\partial J^n}\left[u(t)\frac{\partial S_1}{\partial \psi}\right]^n + \dot{u}(t)S_1 \tag{32}$$

will account for all terms of lower order with respect to $u(t)$ for rotation numbers $1/n$.

For the resonances in the main series, only the terms multiple to odd powers of n should be preserved in expressions for $u^n(t)$, since only these expansions contain the first power of $\cos(\omega_0 + \varphi_0)$. Let us represent $u^n(t)$ as

$$\begin{aligned}
u^n &= u_0^n \sum_{j=0}^{[n/2]} C_n^{2j+1}\mu^{2j+1}\cos^{2j+1}(\omega_0 t + \varphi_0)\\
&= u_0^n \mu\cos(\omega_0 t + \varphi_0)\Phi_n(\mu),
\end{aligned} \tag{33}$$

where

$$\Phi_n(\mu) = \sum_{j=0}^{[n/2]} C_n^{2j+1} C_{2j+1}^{j} \left(\frac{\mu}{2}\right)^{2j},$$

$[A]$ is the integer part of A, and C_i^j are binomial coefficients.

Considering (20) and (33) and averaging (Lichtenberg and Lieberman, 1983; Zaslavsky, 2007), we obtain

$$\overline{\Psi}(J, \psi, t;\ n) = \Psi_0(J) - u_0^n \mu \Phi_n(\mu) \frac{(-1)^{(3n-1)/2}}{2^{n-1} n!} \frac{\partial^n \Psi_0}{\partial J^n} \left[\frac{\sqrt{2J}}{\omega(J)}\right]^n \cos(\omega_0 t + \varphi_0) \sin(n\psi) \tag{34}$$

for the resonance $1/n$ ($n = 3, 5, \ldots$) instead of (32).

Further, by analogy with (25), we obtain the expression for the effective Hamiltonian

$$\widetilde{\Psi}(\Delta J, \phi, t; n) = \frac{1}{2} \frac{\mathrm{d}\omega(J_n)}{\mathrm{d}J} (\Delta J)^2 - u_0^n \mu \Phi_n(\mu) \frac{(-1)^{(3n-1)/2}}{2^{n-1} n!} \frac{\mathrm{d}^{n-1}\omega(J_n)}{\mathrm{d}J^{n-1}} \left[\frac{\sqrt{2J_n}}{\omega(J_n)}\right]^n \cos\phi_n, \tag{35}$$

where

$$\phi_n = n\psi - \omega_0 t - \varphi_0 + \frac{\pi}{2}.$$

Now, using the expression (35), we obtain estimates for the width of the domain of the resonance with multiplicity n in terms of frequency

$$\Delta\omega(J_n) = \sqrt{u_0^n \mu \Phi_n(\mu) \frac{(-1)^{(3n-1)/2}}{2^{n-1} n!} \frac{\mathrm{d}\omega(J_n)}{\mathrm{d}J} \frac{\mathrm{d}^{n-1}\omega(J_n)}{\mathrm{d}J^{n-1}} \left[\frac{\sqrt{2J_n}}{\omega(J_n)}\right]^n} \tag{36}$$

and in terms of action

$$\Delta J_n = \sqrt{\frac{u_0^n \mu \Phi_n(\mu) \mathrm{d}^{n-1}\omega(J_n)/\mathrm{d}J^{n-1} [\sqrt{2J_n}/\omega(J_n)]^n}{2^{n-1} n! \mathrm{d}\omega(J_n)/\mathrm{d}J}}.$$

The distance between the centers of the domains of the nonlinear resonances $1/n$ and $1/(n+2)$ with odd n can now be estimated as

$$|\delta J| \sim \left| \frac{2\omega(J_n)}{(n+2)\mathrm{d}\omega(J_n)/\mathrm{d}J} \right|,$$

and we obtain the estimate for the ratio analogous to (29)

$$K_c = \frac{\Delta J}{2\delta J} \sim \sqrt{\frac{(n+2)^2 u_0^n \mu \Phi(\mu) (\mathrm{d}^{n-1}\omega(J_n)/\mathrm{d}J^{n-1})(\mathrm{d}\omega(J_n)/\mathrm{d}J)[\sqrt{2J_1}/\omega(J_n)]^n}{2^{n-1} n! (2\omega(J_1))^2}}. \tag{37}$$

Fig. 12 gives dependencies of K_c on y for the specified values of perturbation frequencies. These dependencies were constructed in the following manner: (i) resonance values of the action variable were found from equation $\omega(J_n) = \omega_0/n$ for each ω_0, (ii) obtained values were used to determine the appropriate

values of y at $x = 0$, (iii) formula (37) was used to calculate the ratios K_c as functions of y, (iv) curves were drawn on plane (y, K_c) through the points thus obtained.

The exceedance of the level of 1 by the curve $K_c(n, J_n(\omega_0))$ implies that the resonance of multiplicity n completely overlaps the resonance of multiplicity $n+2$, which (being narrower) destroys the resonance of multiplicity n only partially. On the other hand, the width of the resonance domain $n-2$ is not sufficient for its destruction, since the condition $K_c < 1$ is valid for it. As it was shown above, resonances with even multiplicities have higher order in terms of u_0 and do not play any significant part.

Fig. 12 also shows the dependence of K_c on y for the resonance with the rotation number of $\frac{1}{1}$, calculated by using the formula (29). The overlapping criterion for the resonance $\frac{1}{1}$ was calculated with allowance made for the role of $\frac{1}{2}$, i.e., the only even resonance that appears in this system.

These relationships for the overlapping criterion allow us to analyze the specific features of chaotization of the phase space for different perturbation frequencies. Fig. 13 gives Poincaré cross-sections calculated for four characteristic values of the perturbation frequency (corresponding to the curves in Fig. 12).

As can be seen from Fig. 12, at the perturbation frequency of $\omega_0 = 0.5$ the criterion values within the interval $y \subset [-10;\ -5]$ are rather low, which determines the regular character of trajectories. This is confirmed by the appropriate Poincaré cross-section (Fig. 13a). The extent of overlapping increases beyond this interval, and clearly, the chaotization of trajectories takes place. However, since the extent of overlapping at small y does not reach the critical value, the resonances in this domain do not overlap completely. A regular behavior can be expected within linear stability domains (the unit circumference in Poincaré cross-sections). The regularity in this domain can be more reliably identified with the use of cumulative Lyapunov indices (Pierrehumbert, 1991a). According to (9) (see also Izrailsky et al., 2004), the eigenvalues of the linearized matrix can be expressed in a zero approximation in terms of the azimuth velocity:

$$\lambda_{1,2} = \pm \mathrm{i} \sqrt{\frac{1}{r} \frac{\mathrm{d}V^2(r)}{\mathrm{d}r}}. \tag{38}$$

Clearly, the cumulative Lyapunov indices will be imaginary within the linear-stability domain. Obviously, the disturbed trajectories can leave this domain and, hence, accumulate positive values of indices at relatively low perturbations. This mechanism accounts for the chaotization of a small part of the stability domain in the vicinity of the boundary.

According to (38), the derivative of the azimuth velocity changes its sign outside of the linear-stability domain, and the accumulated indices become real. However, as the derivative is small, they are not large. Thus, the chaotization in the vicinity of the linear-stability domain should be weak. This can be also seen from the decreasing values of the overlapping criterion for the resonance $\frac{1}{1}$ as the stability domain is approached (the perturbation frequency increases). As a first approximation, the accumulated indices are small even at sufficiently large r, since the derivative of the azimuth velocity decreases as r^{-2}. The proposed criterion yields qualitatively similar result. However, it is worth mentioning that our estimates are inapplicable in the vicinity of the separatrix, though, as we can see, they adequately reflect the trend.

The chaotization can be seen to increase in the vicinity of the linear-stability domain, but it decreases as the boundary is approached. The motions are regular within the domain. Chaotization can also be seen near the separatrix, though the overlapping criterion allows its boundary to be determined only approximately.

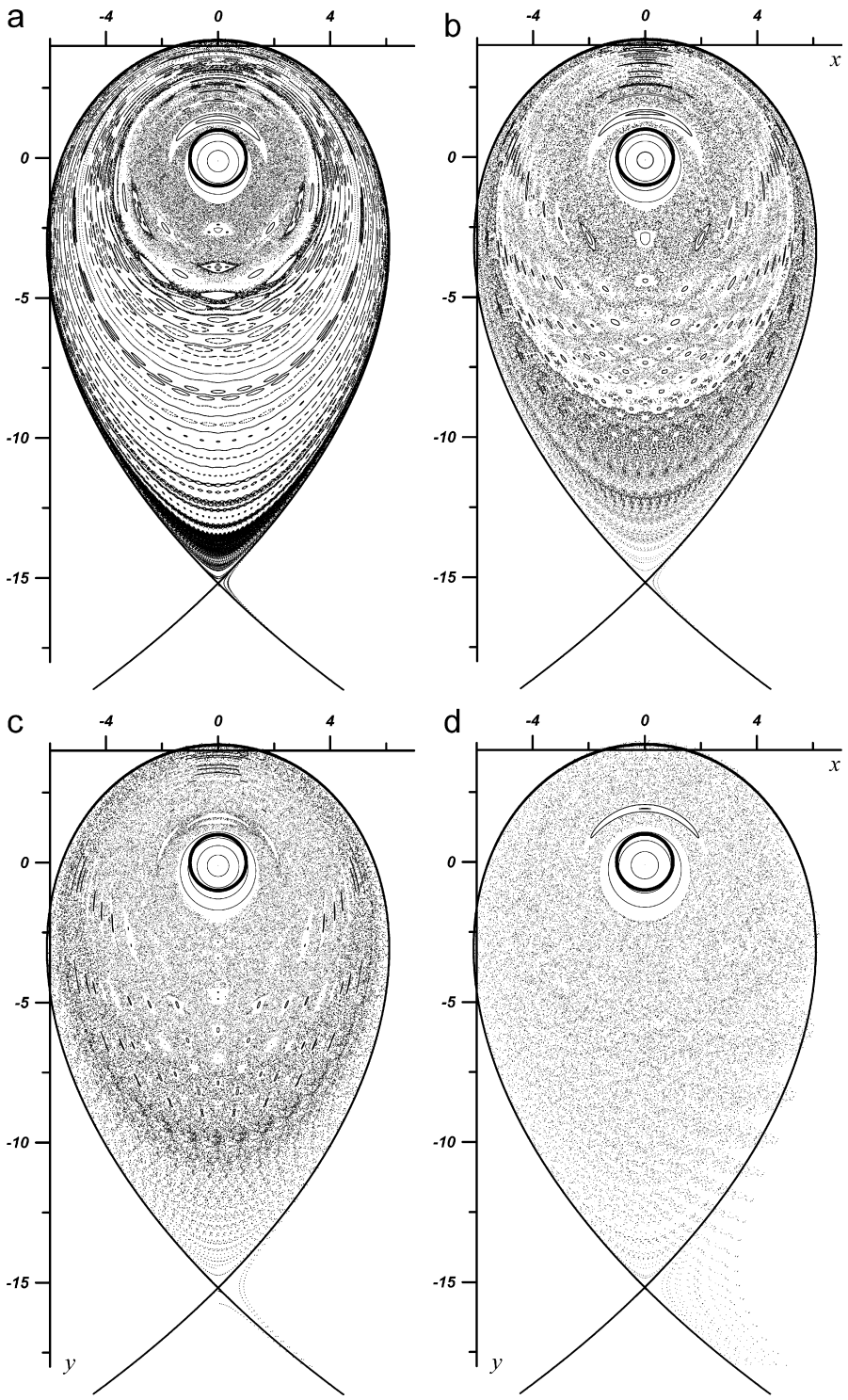

Fig. 13. Poincaré cross-section at $\Omega = 0$, $A = B = 0$, $u_0 = 0.092$, $v_0 = 0$, $\mu = 0.9$, $\varphi_0 = 0$ for the cases: (a) $\omega_0 = 0.5$, (b) $\omega_0 = 0.4$, (c) $\omega_0 = 0.35$, (d) $\omega_0 = 0.25$.

Further we will consider the case of perturbation frequency of 0.4, which is of special interest in some sense. In accordance with the criterion, we see a considerable overlapping of resonances in the stability domain. However, the critical value is not reached here, therefore the resonance of the form $\frac{1}{2}$ is not destroyed completely. At the same time, the ratio K_c cannot predict the destruction of the resonance $\frac{1}{1}$, since this requires the use of a criterion based on the width of the domain of the resonance $\frac{1}{2}$.

The values of the criterion decrease with the distance from the center, and we can see a decrease in the extent of overlapping (chaotization). In the domain of minimum overlapping, we can speak about a stochastic web, since we have thin stochastic layers in the vicinity of the separatrices of nonlinear resonances, which, however, do not overlap. Two interesting phenomena can be seen in this case: dynamic traps and Levy flights (Budyansky et al., 2004a). Detailed analysis of the behavior of a marker that was initially placed in the vicinity of the stability domain shows that it will quickly reach the domain of stochastic web. Indeed, the extent of resonance overlapping within the interval from $y = -2$ to $y = -5$ is quite large, and the islands of regular behavior are separated by large intervals through which the marker can easily move into the external domain. A dark belt can be distinctly seen in the vicinity of the resonance $\frac{1}{9}$ about $y = -5.5$ in Fig. 13b. This belt indicates that the trajectory adheres to this chain of islands, i.e., there are a trap and, accordingly, Levy's flights here. Nevertheless, after some time, the marker moves further and stays for a long time in the domain before a slightly permeable barrier (about $y = -8$), where the stochastic web becomes very thin. Here, the probability for the marker to diffuse into the external domain is small. This is the second trap, though of somewhat different type: the markers become entangled between several nonlinear resonances and rarely penetrate through thin spaces. Levy's flights can also be seen here, though we will not study these in detail. After the penetration through the barrier, the marker adheres to the least destroyed resonance, which maintains the barrier from outside. This is the third trap. Next the particle becomes entangled between partially destroyed resonances in the domain roughly from $y = -9$ to 11. Since the overlapping criterion predicts an increase in the chaotization extent when approaching the separatrix, as is typical of dynamic systems, the marker, after leaving the last trap, rapidly penetrates into the flow-through domain.

Thus, in this case we see the possibility of transport from the vortex center into the flow-through domain; however, because of the presence of at least three traps, the washing-out process is quite slow and is accompanied by intense mixing. It is likely that the criterion value of 0.5 is close to the boundary at which the transport barrier forms. This value corresponds to a weakly permeable domain. A slight drop in it is accompanied by the formation of a KAM-torus, which serves as an impermeable barrier for particle transport.

At high values of the overlapping criterion, the stochastic web near the barrier starts extending. This situation is illustrated by Fig. 13c, where the perturbation frequency is 0.35. According to the criterion, all resonances in the main series, except for $\frac{1}{1}$ should be destroyed, as is the case in the appropriate Poincaré cross-sections. In this situation, the transport of solute from the center of the vortex domain into the flow-through zone becomes quite effective. It is important that the vortex domain is filled with a much higher density then in the case of perturbation frequency of 0.25 (Fig. 13d). This effect is quite explicable: the value of the overlapping criterion either slightly exceeds the critical value or is somewhat less than that, and markers are retained in the vicinity of the stability islands, though not for a long time. As the perturbation frequency decreases further, the minimum value of the overlapping criterion grows substantially above the critical value, and the degree of chaotization increases. As the separatrix is approached, twofold or even greater overlapping of resonances can be expected. Indeed, we can see

much faster export of markers in Fig. 13d (the number of points in the vortex domain is much less). The perturbation frequency of 0.25 can be regarded as optimal for transport, since, in this case, the maximum part of the vortex domain is ventilated. In accordance with the criterion, the overlapping of resonances will increase with a further decrease in the perturbation frequency. This results in a much faster washing out of markers (Kozlov et al., 2005; Izrailsky et al., 2004). The resonance domain $\frac{1}{1}$ will shift even further from the center, however, the widths of the resonance domains of higher orders ($\frac{2}{1}$, $\frac{3}{1}$, $\frac{3}{2}$, etc.) are not sufficiently large for chaotization. As a result, the central regularity domain will extend. This reasoning is confirmed by numerical calculations.

An interesting feature of the last Poincaré cross-section is the fact that it demonstrates a persistent diversity of the homoclinic structure, where the boundary between the vortex and external flow domains reflects the structure of lobes (Wiggins, 2005). Moreover, weakly pronounced manifestations of unstable diversity can be seen in the vicinity of the hyperbolic point. The size of lobes, which increases with decreasing frequency, illustrates the fact (Zaslavsky, 2007) that the small parameter in the application of Melnikov theory is the ratio of the perturbation amplitude to the frequency, rather than the amplitude itself.

Thus, at the given type of dependence of the rotation frequency on the action variable, where the dependence contains a sufficiently long gentle segment in the vicinity of the separatrix, the system has five critical frequencies of perturbation:

- The first frequency corresponds to the beginning of the penetration of the resonance $\frac{1}{1}$ into the central domain of regular behavior; this frequency is equal to $\omega_{01} = 1 - \Delta\omega(J_1)$ at J_1 offset from the boundary by the distance equal to the width of the domain of the resonance $\frac{1}{1}$. This frequency corresponds to the maximum destruction of the central domain of regular behavior. At $\omega = \omega_{01}$, the chaotic domain surrounding the center is sufficiently narrow, and the motions in the most of the vortex domain are regular.
- The second critical frequency corresponds to the critical value of 1 of the overlapping criterion for the resonance $\frac{1}{1}$. As the frequency increases further, curve K_0 starts declining and we enter the vicinity of the linear stability domain, which corresponds to small values of cumulative Lyapunov indices (38). As the frequency increases even further, more nonlinear resonances with sufficiently small n fall within the domain of small Lyapunov indices, and the resonances that follow them will have an ever decreasing width in accordance with the estimate (36). When the value $\omega_{02} \approx 0.4$ is attained, the external boundary of the chaos domain starts shrinking rapidly.
- The third frequency determines the disappearance of the last KAM-torus that separates the center of the vortex and the vicinity of the separatrix. The minimum value of K_0 at this frequency exceeds the value of 0.45, which corresponds to the condition of the complete absence of resonance overlapping. In our case, this frequency is somewhat greater than ω_{02}. Thus, the transport from the vortex center into the flow-through domain becomes possible at $\omega_{03} > 0.4$.
- The following critical frequency corresponds to the bifurcation frequency of global chaos: $\omega_{04} \approx 0.3$. At this frequency the minimum value of the overlapping criterion exceeds the value of 1.0, which corresponds to the complete overlapping of resonances. This is the situation when a large number of regular-behavior islands disappear and the area of the chaotization domain approaches its maximum.
- And, finally, the last frequency corresponds to the maximum area of the chaos domain. In this case, $\omega_{05} = \omega_{\text{opt}} \approx 0.25$, and there appears a balance between the area of the central domain of regular behavior (which somewhat increases as compared with the minimum value because the $\frac{1}{1}$ resonance

domain, which destroys its vicinity, moves further from it) and the area of the regular-behavior island of this resonance. The point is that, with increasing distance from the regular-behavior domain, this resonance starts extending in accordance with estimate (26) with the result that its destruction becomes stronger. When the total area of these regularity domains is minimum, the area of the chaotic sea domain becomes maximum. As an approximation, we can assume that the plateau in the frequency interval from 0.2 to 0.3 corresponds to the maximum chaotization of the phase space.

All these frequencies for Hamiltonians with such frequency characteristic can be found with the use of the proposed overlapping criterion. To do this, we need to know two critical values: the value 1 corresponds to the complete destruction of the resonance that follows the one for which the resonance criterion is evaluated, and the value 0.45 corresponds to the complete absence of overlapping in the minimum. These values were actually obtained from the analysis of Poincaré cross-section. The more accurate determination of critical frequencies requires the use of Chirikov criterion with the involvement of the widths of domains of both resonances, the thicknesses of their stochastic layers, and, maybe, the contribution of higher order resonances and even resonances. In fact, it will be sufficient to take into account both widths of the resonance domains in the main series.

Let us consider the mechanisms that govern the behavior of curves K_c. The most important is the domain between $y = -5$ and -10, where both the rotation frequency of particles and its derivative with respect to the action variable are sufficiently small. According to the estimated distances between the centers of resonance domains, they are widely spaced in this interval. On the other hand, the widths of resonance domains rapidly decrease with increasing n. Thus, there exists a resonance number $n = n^*$ in this domain, starting from which the resonance width is not sufficient for resonances to overlap.

The nonlinearity increases and the distance between resonances decreases in the vicinity of the separatrix (a denumerable number of resonances must exist within the limited interval in separatrix vicinity), i.e., the resonances will again overlap beyond certain distance from the separatrix (this distance can be exponentially small at high frequencies, Neishtadt, 1975, 1984).

Now let us consider the dependence of resonance overlapping on the perturbation frequency. When frequencies are sufficiently high, the domains of resonances with low multiplicities approach the center of the vortex. Therefore, resonances with sufficiently large n and a relatively small width fall within the interval from $y = -5$ to -10. Thus, we can see here either regular or stochastic behavior. As the perturbation frequency decreases, the resonance domains with large n shift toward the separatrix and the resonances with lesser n and larger width occupy their place, so the domain of regular behavior shrinks.

Now let us consider the case when the external flow velocity cannot be considered small. The dependence of the rotation frequency on the distance from the elliptic point for $u_0 = 0.85$ is also given in Fig. 12. Since the derivative of this function is sufficiently large almost everywhere, the situation should resemble the one we have in the previous case in the vicinity of the vortex center. Let us consider some examples of Poincaré cross-sections (Fig. 14) for velocity $u_0 = 0.85$. The characteristic features of the dependence $\omega(y')$ are, on the one hand, the small volume of phase space in terms of frequency and action and, on the other hand, the large values of the derivative of the rotation frequency with respect to action, which increase up to infinity with approaching the separatrix. When the perturbation frequency is small, the largest nonlinear resonance $\frac{1}{1}$ lies far enough from the vortex center and has a moderate width, since the derivative of the rotation frequency is large. For the same reason, the distance between the resonances in the main series is sufficiently large (greater than the width of the resonance domain). It can be expected that a stochastic layer will appear in the vicinity of separatrix and a sufficiently large regular domain will

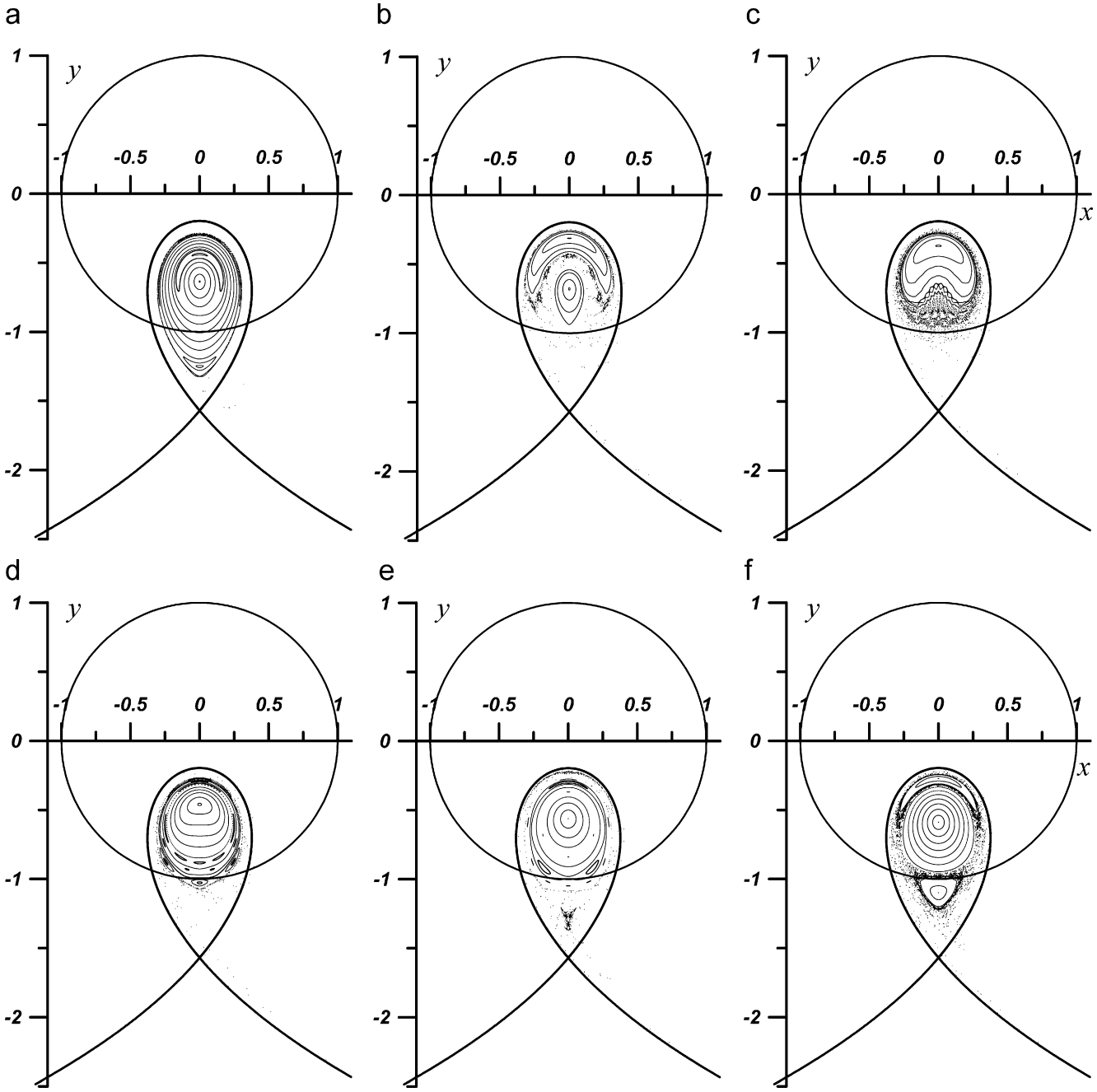

Fig. 14. Poincaré cross-section at $\Omega = 0$, $A = B = 0$, $u_0 = 0.85$, $v_0 = 0$, $\mu = 0.02$, $\varphi_0 = 0$ for the cases: (a) $\omega_0 = 0.5$, (b) $\omega_0 = 0.9$, (c) $\omega_0 = 1.0$, (d) $\omega_0 = 1.1$, (e) $\omega_0 = 1.3$, (f) $\omega_0 = 1.65$.

appear in the vicinity of the center. The size of the regular domain is determined by the position of the resonance $\frac{1}{1}$, since resonances $m/1$ are sufficiently narrow and lie in the domain close to the boundary of linear stability. This is the situation we see in Fig. 14a. Starting from the position in the domain of the resonance $\frac{1}{1}$ and up to the separatrix, markers are rapidly carried out into the external flow domain, while the regular domain contains resonances $\frac{2}{1}$—from one island, and $\frac{3}{2}$—from two islands, the widths of

which are not sufficient for overlapping. Therefore, the behavior of trajectories here is regular. Note that the boundary between the chaotic layer and the regular domain is very abrupt, which is due to the large derivative of the rotation frequency with respect to action. With increasing perturbation frequency, the domain of the resonance $\frac{1}{1}$ approaches the center of the vortex and extends, while the regularity domain shrinks. It is significant that the distance between the resonances $\frac{1}{1}$ and $\frac{1}{2}$ is relatively large; therefore, the former is not destroyed until it is absorbed by the linear stability domain.

Figs. 14b–d show the process of the domain of the resonance $\frac{1}{1}$ approaching the domain of linear stability, which is being destroyed by this resonance, first, partially and next completely. Thus, with the given dependence of frequency on action, there exists only one critical frequency that can be roughly taken as the frequency corresponding to the position of the nonlinear resonance domain such that its distance from the boundary of the linear stability zone is equal to its width. The interval of perturbation frequencies [0.85, 1] can be considered optimal for the chaotization of the vortex domain. In this case, the boundary of the linear stability domain ($y = -1$) corresponds to the frequency of 0.9. The frequency further increasing, the largest resonance $\frac{1}{1}$ disappears from the system (Fig. 14d), and the fractional resonances $\frac{5}{6}$, $\frac{4}{5}$, $\frac{3}{4}$ appear, consisting of 6, 5, and 4 islands, respectively. The width of these resonances is insufficient for their overlap. The boundary of the chaotic domain was determined by the position of the next main resonance series $\frac{1}{2}$, so we obtain a slowly decreasing chaotic domain (below the optimum level).

Figs. 14d and e show the degree of chaotization to be approximately the same. It seems likely that a situation analogous to that considered in studies (Izrailsky et al., 2006; Koshel and Stepanov, 2006), where there exist a local maximum of the degree of chaotization of the vortex domain, can form.

In Fig. 14e, the resonance $\frac{1}{2}$ has already started manifesting itself, since, approaching to the vortex center with increasing frequency, it increases its distance from the resonance of the main series $\frac{1}{3}$, which follows it. However, with approaching the boundary of the linear stability domain, the resonance starts destroying it. Fig. 14f illustrates the beginning of the process of absorption of this resonance by the linear stability domain. The perturbation frequency of 1.65 can be considered critical for this resonance, and its meaning is the same as for the frequency of 0.85 for the resonance $\frac{1}{1}$. After the disappearance of the resonance $\frac{1}{2}$ (or its complete absorption by the domain of linear stability), the degree of chaotization decreases, and the boundary of the domain of regular behavior is controlled by the position of the next resonance in the main series $\frac{1}{3}$. At very high frequencies, the widths of the resonance domains that persist in the system will be small because of larger multiplicities and orders. Now these resonances will not be able to overlap at certain distance from the separatrix, and the width of the stochastic layer will exponentially decrease with increasing perturbation frequency (Neishtadt, 1975, 1984).

Thus, we can conclude that in the vicinity of the optimal frequencies, i.e., the frequencies corresponding to the position of large resonances (in our case, these are $\frac{1}{1}$ and $\frac{1}{2}$), these are the resonances that play the decisive role in the chaotization of the trajectories of the system in the zone between the separatrix and the linear stability domain. This essentially simplifies the qualitative and often the quantitative analysis of the system.

4. Conclusion

The situation discussed in this study can be regarded as very typical in some sense. A relatively simple model of the flow field, which results in simple motion of the trajectories of conservative markers (fluid

particles) under very simple unsteady perturbations, yields a very complicated behavior of trajectories. It is shown that the behavior of trajectories, commonly referred to as "chaotic advection", can cause not only intense mixing or transport of a solute (or other conservative characteristics of the fluid) but also radical changes in the general flow pattern.

Within the framework of the concept of background flows, we considered a vortex flow generated by the interaction between an external flow, either unidirectional or rotating, with an isolated submarine elevation. Clearly, the approach, which is based on the assumption that the potential vorticity is constant, is limited. Nevertheless, it enables the construction of simple dynamically consistent models, which, on the one hand, almost always admit a chaotic advection and, on the other hand, adequately reveal the characteristic features of real geophysical flows.

In fact, we consider the motion of fluid particles in a steady solution within the vicinity of a Taylor column. However, it was found that, in a steady (circular) external flow, there can form two topographic vortices, rotating about the rotation center of the external flow. However, this is not the most significant effect that was found in this model.

It was shown that any deviation from the steady condition, i.e., assuming the external flow to be elliptical, moving the rotation center relative to the submarine elevation, or varying the external flow velocity, results in essential nonsteady Eulerian velocity field. Thus, the system of advection equations, which can be regarded as a dynamic system, becomes nonautonomous, and, accordingly, nonintegrable. Two essentially different situations are possible in this case:

- In the case of a unidirectional flow, the dynamic system becomes open; beyond the separatrix that limits the vortex domain, all streamlines of the undisturbed system pass to infinity; and the chaotization is possible only in the vortex domain. Depending on the model parameters, we can observe
  - purely through flow—at velocities greater than the maximum azimuth velocity of the vortex generated by topography;
  - a small-volume vortex, which becomes chaotic due to the extension of the stochastic domain near the separatrix;
  - or a large-volume vortex at small external flow velocities.

  The latter situation is of great interest, and, as far as we know, has not been studied. In this case, even at sufficiently small amplitudes of the unsteady perturbation of velocity, two chaotic-behavior domains form in the vortex domain. In this case, these represent a relatively narrow near-separatrix layer and a chaotization domain in the vicinity of the vortex center. The central domain assures good mixing, while the near-separatrix domain assures good transport to the external flow area, i.e., vortex ventilation. A domain of weak nonlinearity, which lies between these domains, forms a barrier for the chaotic transport from the vortex center to the external flow domain.

  It is shown that in this situation, a simple qualitative description is possible. The consideration of an undisturbed steady system shows that the rotation frequency of trajectories about the elliptic point varies rapidly (strong nonlinearity) in the vicinity of a center; next, there exists a domain where this characteristic varies slowly (weak nonlinearity, quasi-regular behavior); and the rotation frequency in the vicinity of the separatrix again varies rapidly (strong nonlinearity). The same characteristic (rotation frequency), at a given perturbation frequency, determines the position, multiplicities, and intensities of nonlinear resonances. The quasi-regular or chaotic behavior was found to be determined by the position and the extent of overlapping of a very small number of sufficiently large nonlinear resonances. By changing the perturbation frequency, we can control the distribution of these resonances

and their intensities. Thus, this mechanism allows us to obtain the criteria of existence and the positions of quasi-regular barriers or their destruction, including the values of model parameters that are optimal for mixing or chaotic transport.

- In the case of a flow rotating along an ellipse, the same mechanism allows us to identify somewhat different effects. The system becomes closed, and the stream lines around the separatrix of topographic vortices are closed. This means that nonlinear resonances can also form beyond the separatrix. Two analogies are possible at small perturbations: (1) the ellipticity of a tidal stream is equivalent to an unsteady perturbation on the double rotation frequency of the external flow; (2) the displacement of the rotation center relative the submarine elevation is equivalent to a perturbation on the rotation frequency.

  Because of the rotation of the external flow, the fluid motion at large distances form the submarine elevation is close to the solid-body rotation. This determines the existence of a narrow interval in the rotation frequencies of fluid particles and results in a situation, when only a small number of nonlinear resonances can exist in the system. These are mostly fractional resonances from a small number of islands of regular behavior. Such resonance structures can be interpreted as chains of vortices-satellites, which surround the chaotic central domain. Thus, in the case of an elliptic perturbation, we obtain a well mixed vortex core, which is much greater than steady topographic vortices. Vortex structures that are not completely destroyed can exist within this cloud of chaotic trajectories (remains of nonlinear resonances). Analogous structures, though with a larger number of vortices, form at the periphery of the mixed domain. In the case where the perturbation frequencies are not multiples of the rotation frequency, the situation becomes much more complicated. Because of the presence of trajectories with the maximum rotation frequency in the external domain, pairs of resonances with equal multiplicities will form with a barrier, consisting of regular trajectories, between them. The latter will destroy at certain values of the perturbation frequency that correspond to the reconnect of these resonances in the vicinity of the trajectory with the maximum rotation frequency.

  It is important that, since the behavior of disturbed trajectories in the external domain is determined by a small number of nonlinear resonances, the analysis of the scenarios of chaotization, mixing, and transport of the solute becomes a relatively simple task. Having constructed (analytically or numerically) the dependence of the rotation frequency of fluid particles on the distance to the center of the vortex in the undisturbed system, one can determine the position and intensity of nonlinear resonances given the perturbation parameters. This procedure allows one to determine whether there are any barriers or transport corridors from the central vortex zone into the external domain and evaluate the size of the chaotization domain.

The non-dimensionalization of model variables was based on the scales corresponding to the synoptic times of flow variations; this corresponds to Pierrehumbert hypothesis (1991a) regarding the efficiency of chaotic mixing and transport at small perturbation frequencies. However, at small velocities, when the chaotization can form at considerable frequencies, one can obtain dimensional values, corresponding to some tidal harmonics, such as shelf waves with a two-day period, which become stronger in the vicinity of the elevation.

We would like to note that this barotropic quasi-geostrophic model may be applied only to small obstacles; diapycnal mixing cannot be directly investigated in this framework. It is possible to study the effect of a finite height hill in a two-layer model when the obstacle penetrates into the upper layer. Then we can consider the lower-layer incident flow to round an island; and in the upper layer it represents a

small obstacle. Such a method was used, for example, in the work by Thompson (1993), and we suggest in future realizing similar ideas in the problem of chaotic advection in a stratified flow.

Acknowledgments

We are grateful to Hassan Aref and Ziv Kizner for useful discussion. This study was supported by RFBR (projects 07-05-00452, 07-05-92210 and 08-05-00061), INTAS-AIRBUS (project 04-80-7297), and Far-East Division, RAS (project 05-I-P13-048). The study was carried out within the framework of GDRE "Regular and chaotic hydrodynamics".

References

Abraham, E.R., Bowen, M.M., 2002. Chaotic stirring by a mesoscale surface-ocean flow. Chaos 12 (2), 373–381.
Allen, J.S., Samelson, R.M., Newberger, P.A., 1991. Chaos in a model of quasigeostrophic flow over topography: an application of Melnikov's method. J. Fluid Mech. 226, 511–547.
Angilella, J.S., Brancher, J.P., 2003. Note on chaotic advection in an oscillating drop. Phys. Fluids 15 (1), 261–264.
Aref, H., 1984. Stirring of chaotic advection. J. Fluid Mech. 143, 1–21.
Aref, H., 1990. Chaotic advection of fluid particles. Phil. Trans. R. Soc. Lond. A 333 (1631), 273–288.
Aref, H., 2002. The development of chaotic advection. Phys. Fluids 14 (4), 1315–1325.
Aref, H., Balachandar, S., 1986. Chaotic advection in a Stokes flow. Phys. Fluids 29 (11), 3515–3521.
Aref, H., Pomphrey, N., 1982. Integrable and chaotic motions of four vortices. I. The case of identical vortices. Proc. R. Soc. Lond. A 380, 359–387.
Babiano, A., Boffetta, G., Provenzale, A., Vulpiani, A., 1994. Chaotic advection in point vortex models and two-dimensional turbulence. Phys. Fluids 6 (7), 2465–2474.
Balasuriya, S., Jones, C.K.R.T., 2001. Diffusive draining and growth of eddies. Nonlinear Processes in Geophys. 8 (4–5), 241–251.
Beerens, S.P., Ridderinkhof, H., Zimmerman, J.F.E., 1994. An analytical study of chaotic stirring in tidal areas. Chaos Solitons and Fractals 4 (6), 1011–1029.
Bjerknes, J., 1966. A possible response of the atmospheric Hadley circulation to equatorial anomalies of ocean temperature. Tellus 18 (4), 820–829.
Bjerknes, J., 1969. Atmospheric teleconnections from the equatorial Pacific. Mon. Weather Rev. 97 (3), 163–172.
Boffetta, G., Celani, A., Franzese, P., 1996. Trapping of passive tracers in a point vortex system. J. Phys. A 29, 3749–3759.
Borisov, A.V., Mamaev, I.S., 2005. Mathematical methods of dynamics of vortex structures. Inst. Comput. Sci., Moscow-Izhevsk, 368p.
Borisov, A.V., Kilin, A.A., Mamaev, I.S., 2005. Reduction and chaotic behavior of point vortices on plane and sphere. Russian Sci. J. Nonlinear Dyn. 1 (2), 233–246.
Bower, A.S., 1991. A simple kinematic mechanism for mixing fluid parcels across a meandering jet. J. Phys. Oceanogr. 21 (1), 173–180.
Bower, A.S., Rossby, H.T., Lillibridge, J.L., 1985. The Gulf Stream—barrier or blender? J. Phys. Oceanogr. 15 (1), 24–32.
Bracco, A., Provenzale, A., Scheuring, I., 2000. Mesoscale vortices and the padadox of the plancton. Proc. Roy. Soc. Lond. B. 267, 1795–1800.
Brown, M.G., Samelson, R.M., 1994. Particle motion in vorticity-conserving, two-dimensional incompressible flows. Phys. Fluids 6 (9), 2875–2876.
Budyansky, M.V., Uleysky, M.Yu., Prants, S.V., 2002. Fractals and dynamic traps in the simplest model of chaotic advection with a topographic vortex. Dokl. Earth Sci. 387, 929–932.
Budyansky, M.V., Uleysky, M.Yu., Prants, S.V., 2004a. Chaotic scattering, transport, and fractals in a simple hydrodynamic flow. J. Exp. Theor. Phys. 99 (5), 1018–1027.
Budyansky, M.V., Uleysky, M.Yu., Prants, S.V., 2004b. Hamiltonian fractals and chaotic scattering of passive particles by a topographical vortex and an alternating current. Physica D 195, 369–378.

Budyansky, M.V., Uleysky, M.Yu., Prants, S.V., 2007. Lagrangian coherent structures, transport and chaotic mixing in simple kinematic ocean models. Comm. Nonlinear Sci. Numer. Simul. 12, 31–44.

del-Castillo-Negrete, D., Morrison, P.J., 1993. Chaotic transport by Rossby waves in shear flow. Phys. Fluids A 5 (4), 948–965.

Chaiken, J., Chu, C.K., Tabor, M., Tan, Q.M., 1987. Lagrangian turbulence and spacial complexity in a Stokes flow. Phys. Fluids 30 (3), 687–694.

Chirikov, B.V., 1979. A universal instability of many-dimensional oscillator systems. Phys. Rep. 52 (5), 263–379.

Coulliette, C., Wiggins, S., 2001. Intergyre transport in a wind-driven, quasigeostrophic double gyre: an application of lobe dynamics. Nonlinear Processes Geophys. 8 (1), 69–94.

Cox, S.M., Drazin, P.G., Ryrie, S.C., Slater, K., 1990. Chaotic advection of irrotational flows and of waves in fluids. J. Fluid Mech. 214, 517–534.

Dahleh, M.D., 1992. Exterior flow of the Kida ellipse. Phys. Fluids A 4 (9), 1979–1985.

Duan, J., Wiggins, S., 1996. Fluid exchange across a meandering jet with quasiperiodic variability. J. Phys. Oceanogr. 26 (7), 1176–1188.

Duane, G.S., 1977. Synchronized chaos in extended systems and meteorological teleconnections. Phys. Rev. E 56, 6475–6493.

Duane, G.S., Tribbia, J.J., 2001. Synchronized chaos in geophysical fluid dynamics. Phys. Rev. Lett. 86 (19), 4298–4301.

Duane, G.S., Tribbia, J.J., 2004. Weak Atlantic-Pacific teleconnections as synchronized chaos. J. Atmos. Sci. 61 (17), 2149–2168.

Duane, G.S., Webster, P.J., Weiss, J.B., 1999. Co-occurrence of Northern and Southern Hemisphere blocks as partially synchronized chaos. J. Atmos. Sci. 56 (24), 4183–4205.

Eckart, C., 1948. An analysis of the stirring and mixing processes in incompressible fluid. J. Mar. Res. 7 (3), 265–275.

Eckhardt, B., Aref, H., 1988. Integrable and chaotic motions of four vortices. II. Collision dynamics of vortex pairs. Phil. Trans. R. Soc. Lond. A 326, 655–696.

Friedland, L., 1999. Control of Kirchhoff vortices by a resonant strain. Phys. Rev. E 59 (4), 4106–4111.

Goldner, D.R., Chapman, D.C., 1997. Flow and particle motion induced above a tall seamount by steady and tidal background currents. Deep-Sea. Res. I 44 (5), 719–744.

Grote, M.L., 1999. Dynamic mean flow and small-scale interaction through topographic stress. J. Nonlinear Sci. 9 (1), 89–130.

Gryanik, V.M., Sokolovskiy, M.A., Verron, J., 2006. Dynamics of heton-like vortices. Reg. Chaot. Dyn. 11 (3), 383–434.

Gudimenko, A.I., 2007. Chaos and resonances in a rotating flow disturbed by a periodic motion of a point vortex. Russian Sci. J. Nonlinear Dyn. 3 (1), 33–48.

von Handerberg, J., Fraedrich, K., Lunkeit, F., Provenzale, A., 2000. Transient chaotic mixing during a baroclinic life cycle. Chaos 10 (1), 122–134.

Hart, J.E., 1979. Barotropic quasi-geostrophic flow over anisotropic mountains. J. Atmos. Sci. 36 (9), 1736–1746.

Howard, J.E., Hohs, S.M., 1984. Stochasticity and reconnection in Hamiltonian systems. Phys. Rev. A 29 (1), 418–421.

Huppert, H.E., Bryan, K., 1976. Topographically generated eddies. Deep-Sea Res. 23 (8), 655–679.

Ingersoll, A.P., 1969. Inertial Taylor columns and Jupiter's Great Red Spot. J. Atmos. Sci. 26 (7), 744–752.

Izrailsky, Yu.G., Kozlov, V.F., Koshel, K.V., 2004. Some specific features of chaotization of the pulsating barotropic flow over elliptic and axisymmetric seamounts. Phys. Fluids 16 (8), 3173–3190.

Izrailsky, Yu.G., Koshel, K.V., Stepanov, D.V., 2006. Determining the optimal frequency of perturbation in the problem of chaotic transport of particles. Dokl. Phys. 51 (4), 219–222.

Johnson, E.R., 1977. Stratified Taylor columns on a beta plane. Geophys. Astrophys. Fluid Dyn. 9 (2), 159–177.

Johnson, E.R., 1983. Taylor columns in horizontally sheared flow. Geophys. Astrophys. Fluid Dyn. 24, 143–164.

Kawakami, A., Funakoshi, M., 1999. Chaotic motion of fluid particles around a rotating elliptic vortex in a linear shear flow. Fluid Dyn. Res. 25, 167–193.

Kennelly, M.A., Evans, R.H., Joyce, T.M., 1985. Small-scale cyclones on the periphery of Gulf Stream warm-core rings. J. Geophys. Res. 90 (5), 8845–8857.

Koh, T.-Y., Legras, B., 2002. Hyperbolic lines and the stratospheric polar vortex. Chaos 12 (2), 382–394.

Koshel, K.V., Prants, S.V., 2006. Chaotic advection in the ocean. PHYS-USP 49 (11), 1151–1178.

Koshel, K.V., Stepanov, D.V., 2005. Boundary effect on the mixing and transport of passive impurities in a nonstationary flow. Tech. Phys. Lett. 31 (2), 135–137.

Koshel, K.V., Stepanov, D.V., 2006a. Chaotic advection in two layers flow above the isolated bottom obstacle: the role of unsteady-perturbation frequency. Russian Sci. J. Nonlinear Dyn. 2 (2), 147–164.

Koshel, K.V., Stepanov, D.V., 2006b. Chaotic advection induced by a topographic vortex in baroclinic ocean. Dokl. Earth Sci. 407 (3), 455–459.
Kozlov, V.F., 1983. Models of topographic eddies in ocean. Nauka, Moscow, 200p.
Kozlov, V.F., 1995. Background currents in geophysical hydrodynamics. Izvestia, Atmos. Oceanic Phys. 31 (2), 245–250.
Kozlov, V.F., Koshel, K.V., 1999. Barotropic model of chaotic advection in background flows. Izvestia, Atmos. Oceanic Phys. 35 (1), 123–130.
Kozlov, V.F., Koshel, K.V., 2000. A model of chaotic transport in the barotropic background flow. Izvestia, Atmos. Oceanic Phys. 36 (1), 109–118.
Kozlov, V.F., Koshel, K.V., 2001. Some features of chaos development in an oscillatory barotropic flow over an axisymmetric submerged obstacle. Izvestia, Atmos. Oceanic Phys. 37 (3), 351–361.
Kozlov, V.F., Koshel, K.V., 2003. Chaotic advection in models of background currents of geophysical hydrodynamics. In: Borisov, A.V., Mamaev, I.S., Sokolovskiy, M.A., Moscow-Izhevsk, (Eds.), Fundamental and applied problems of vortex theory. pp. 471–504.
Kozlov, V.F., Sokolovskiy, M.A., 1980. Influence of cylindrical topographic disturbances on an unsteady zonal flow of a stratified fluid on the beta plane. Izvestia, Atmos. Oceanic Phys. 16 (8), 596–604.
Kozlov, V.F., Sokolovskiy, M.A., 1981. Meander of barotropic zonal current crossing a bottom ridge (periodic regime). Oceanology 21 (6), 684–687.
Kozlov, V.F., Koshel, K.V., Stepanov, D.V., 2005. Influence of the boundary on chaotic advection in the simplest model of a topographic vortex. Izvestia, Atmos. Oceanic Phys. 41 (2), 217–227.
Kuebel Cervantes, B.T., Allen, J.S., Samelson, R.M., 2004. Lagrangian characteristics of continental shelf flows forced by periodic wind stress. Nonlinear Processes Geophys. 11 (1), 3–16.
Kuznetsov, L., Zaslavsky, G.M., 1998. Regular and chaotic advection in the flow field of a three-vortex system. Phys. Rev. E 58 (6), 7330–7349.
Kuznetsov, L., Zaslavsky, G.M., 2000. Passive particle transport in three-vortex flow. Phys. Rev. E 61 (4), 3777–3792.
Kuznetsov, L., Toner, M., Kirwan, A.D., Jones, C.K.R.T., Kantha, L.H., Choi, J., 2002. The loop current and adjacent rings delineated by Lagrangian analysis of the near-surface flow. J. Mar. Res. 60 (3), 405–429.
Landau, L.D., Lifshits, E.M., 2004. Course of theoretical physics. vol. 1: Mechanics. Third ed., Pergamon Press, Oxford, 198p.
Leoncini, X., Zaslavsky, G.M., 2002. Jets, stickiness, and anomalous transport. Phys. Rev. E 65 (4), 046216-1–046216-16.
Leoncini, X., Kuznetsov, L., Zaslavsky, G.M., 2000. Motion of three vortices near collapse. Phys. Fluids 12 (8), 1911–1927.
Leoncini, X., Kuznetsov, L., Zaslavsky, G.M., 2001. Chaotic advection near a three-vortex collapse. Phys. Rev. E 63 (3), 036224-1–036224-17.
Lichtenberg, A., Lieberman, M., 1983. Regular and Stochastic Motion. Springer, New York. 516p.
Liu, Z., Yang, H., 1994. The intergure chaotic transport. J. Phys. Oceanogr. 24 (8), 1768–1782.
Llewellyn Smith, S.G., Tobias, S.M., 2004. Vortex dynamos. J. Fluid Mech. 498, 1–21.
Loder, J.W., Shen, Y., Ridderinkhof, H., 1997. Characterization of three-dimensional Lagrangian circulation associated with tidal rectification over a submarine bank. J. Phys. Oceanogr. 27 (8), 1729–1742.
Lozier, M.S., Pratt, L.J., Rogerson, A.M., Miller, P.D., 1997. Exchange geometry revealed by float trajectories in the Gulf Stream. J. Phys. Oceanogr. 27 (11), 2327–2341.
Maas, L.R.M., Doelman, A., 2002. Chaotic tides. J. Phys. Oceanogr. 32 (3), 870–890.
Malhotra, N., Wiggins, S., 1998. Geometric structures, lobe dynamics, and Lagrangian transport in flows with aperiodic time-dependence, with applications to Rossby wave flow. Nonlinear Sci. 8, 401–456.
Mancho, A.M., Small, D., Wiggins, S., 2004. Computation of hyperbolic trajectories and their stable and unstable manifolds for oceanographic flows represented as data sets. Nonlinear Processes in Geophys. 11 (1), 17–33.
Mancho, A.M., Small, D., Wiggins, S., 2006. A tutorial on dynamical systems concepts applied to Lagrangian transport in oceanic flows defined as finite time data sets: theoretical and computational issues. Phys. Rep. 437 (3–4), 55–124.
Marshall, J.S., 1995. Chaotic oscillations and breakup of quasi-geostrophic vortices in the N-layer approximation. Phys. Fluids 7 (5), 983–992.
Meleshko, V.V., Aref, H., 1996. A blinking rotlet model for chaotic advection. Phys. Fluids 8 (12), 3215–3217.
Meleshko, V.V., Konstantinov, M.Yu., 1993. Dynamics of vortex structures. Naukova Dumka, Kiev, 280p.
Meleshko, V.V., Konstantinov, M.Yu., Gurzhi, A.A., Konovaljuk, T.P., 1992. Advection of a vortex pair atmosphere in a velocity field of point vortices. Phys. Fluids A 4 (12), 2779–2797.
Meyers, S.D., 1994. Cross-frontal mixing in a meandering jet. J. Phys. Oceanogr. 24 (7), 1641–1646.

Miller, P.D., Pratt, L.J., Helfrich, K.R., Jones, C.K.R.T., 2002. Chaotic transport of mass and potential vorticity for an island recirculation. J. Phys. Oceanogr. 32 (1), 80–102.
Mizuta, R., Yoden, S., 2001. Chaotic mixing and transport barriers in an idealized stratospheric polar vortex. J. Atmos. Sci. 58 (17), 2616–2629.
Neishtadt, A.I., 1975. Passage through a separatrix in a resonance problem with a slowly-varying parameter. Prikl. Mat. Meh. 39 (4–6), 1331–1334.
Neishtadt, A.I., 1984. The separation of motions in systems with rapidly rotating phase. P.M.M. USSR 48, 133–139.
Neu, J.C., 1984. The dynamics of a columnar vortex in an imposed strain. Phys. Fluids 27 (10), 2397–2402.
Ngan, K., Shepherd, T.G., 1997. Chaotic mixing and transport in Rossby-wave critical layer. J. Fluid. Mech. 334, 315–351.
Ngan, K., Shepherd, T.G., 1999a. A closer look at chaotic advection in the stratosphere. Part I: geometric structure. J. Atmos. Sci. 56 (24), 4134–4152.
Ngan, K., Shepherd, T.G., 1999b. A closer look at chaotic advection in the stratosphere. Part II: statistical diagnostics. J. Atmos. Sci. 56 (24), 4153–4166.
Novikov, E.A., 1975. Dynamics and statistics of a system of vortices. Z. Eksp. Teor. Fiz. 68, 1868–1882.
Novikov, E.A., Sedov, Yu.B., 1978. Stochastic properties of a four-vortex system. Z. Eksp. Teor. Fiz. 75, 868–876.
Nycander, J., Döös, K., Coward, A.C., 2002. Chaotic and regular trajectories in the Antarctic Circumpolar Current. Tellus 54 A (1), 99–106.
Paldor, N., Boss, E., 1994. Chaotic trajectories of tidally perturbed internal oscillations. J. Atmos. Sci. 49 (23), 2306–2318.
Pasmanter, R.A., 1991. Anomalous diffusion and patchiness generated by Lagrangian chaos in shallow tidal flows. Phys. Fluids A 3 (5), 1441.
Péntek, A., Tél, T., Toroczkai, T., 1995. Chaotic advection in the velocity field of leapfrogging vortex pairs. J. Phys. A 28 (8), 2191–2216.
Pierce, R.B., Fairlie, T.D.A., 1993. Chaotic advection in the stratosphere: implications for the dispersal of chemically perturbed air from the polar vortex. J. Geophys. Res. 98 (D10), 18589–18596.
Pierce, R.B., Fairlie, T.D., Grose, W.L., Swinbank, R., O'Neil, A., 1994. Mixing processes within the polar night jet. J. Atmos. Sci. 51 (20), 2957–2972.
Pierrehumbert, R.T., 1991a. Large-scale horizontal mixing in planetary atmospheres. Phys. Fluids A 3 (5), 1250–1260.
Pierrehumbert, R.T., 1991b. Chaotic mixing of tracer and vorticity by modulated travelling Rossby waves. Geophys. Astrophys. Fluid Dyn. 58, 285–319.
Pierrehumbert, R.T., Yang, H., 1993. Global chaotic mixing on isentropic surfaces. J. Atmos. Sci. 50 (15), 2462–2480.
Poje, A.C., Haller, G., 1999. Geometry of cross-stream mixing in a double-gyre ocean model. J. Phys. Oceanogr. 29 (8), 1649–1665.
Polvani, L.M., Plumb, R.A., 1992. Rossby wave breaking, microbreaking, filamentation, and secondary vortex formation: the dynamics of a perturbed vortex. J. Atmos. Sci. 49 (6), 462–476.
Polvani, L.M., Wisdom, J., 1990. Chaotic Lagrangian trajectories around an elliptical vortex parch embedded in a constant and uniform background shear flow. Phys. Fluids A 2 (2), 123–126.
Prants, S.V., Budyansky, M.V., Uleysky, M.Yu., Zaslavsky, G.M., 2006. Chaotic mixing and transport in a meandering jet flow. Chaos 16 (3), 033117-1–033117-8.
Pratt, L.J., Lozier, M.G., Belyakova, N., 1995. Parcel trajectories in quasigeostrophic jets: neutral models. J. Phys. Oceanogr. 25 (6), 1451–1466.
Raynal, F., Wiggins, S., 2006. Lobe dynamics in a kinematic model of a meandering jet. I. Geometry and statistics of transport and lobe dynamics with accelerated convergence. Physica D 223, 7–25.
Ridderinkhof, H., Loder, J.W., 1994. Lagrangian characterization of circulation over submarine banks with application to the Outer Gulf of Marine. J. Phys. Oceanogr. 24 (6), 1184–1200.
Ridderinkhof, H., Zimmerman, J.T.F., 1992. Chaotic stirring in a tidal system. Science 258, 1107–1111.
Rogerson, A.M., Miller, P.D., Pratt, L.J., Jones, C.K.R.T., 1999. Lagrangian motion and fluid exchange in a barotropic meandering jet. J. Phys. Oceanogr. 29 (10), 2635–2655.
Rom-Kedar, V., Poje, A.C., 1999. Universal properties of chaotic transport in the presence of diffusion. Phys. Fluids 11 (8), 2044–2057.
Sakamoto, K., Akitomo, K., 2006. Instabilities of the tidally induced bottom boundary layer in the rotating frame and their mixing effect. Dyn. Atmos. Oceans 41 (3–4), 191–219.
Samelson, R.M., 1992. Fluid exchange across a meander jet. J. Phys. Oceanogr. 22 (4), 431–440.

Samelson, R.M., Allen, J.S., 1987. Quasi-geostrophic topographical generated mean flow over the continental margin. J. Phys. Oceanogr. 17 (11), 2043–2064.
Simiu, E., 1969. Melnikov process for stochastically perturbed, slowly varying oscillators: application to a model of wind-driven coastal currents. J. Appl. Mech. 63 (2), 429–435.
Sokolovskiy, M.A., Zyryanov, V.N., Davies, P.A., 1988. On the influence of an isolated submerged obstacle on a barotropic tidal flow. Geophys. Astrophys. Fluid Dyn. 88 (1), 1–30.
Solomon, T.H., Weeks, E.R., Swinney, H.L., 1994. Chaotic advection in a two-dimensional flow: Lévy flights and anomalous diffusion. Physica D. 74, 70–84.
Stirling, J.R., 2003. Chaotic advection, transport and patchiness in clouds of pollution in an estuarine flow. Discrete Contin. Dyn. Syst. Ser. B. 3 (2), 263–284.
Stolovitsky, G., Kaper, T.J., Sirovich, L., 1995. A simple model of chaotic advection and scattering. Chaos 5 (4), 671–686.
de Swart, H.E., de Jonge, V.N., Vosbeek, M., 1997. Application of the tidal random walk model to calculate water dispersion coefficients in the Ems Estuary. Est. Coast. Shelf Sci. 45, 123–133.
Thompson, L., 1993. Two-layer quasigeostrophic flow over finite isolated topography. J. Phys. Oceanogr. 23 (7), 1297–1314.
Vainshtein, D.L., Vasiliev, A.A., Neishtadt, A.I., 1996. Changes in the adiabatic invariant and streamline chaos in confined incompressible Stokes flow. Chaos 6 (1), 67–77.
Velasco Fuentes, O.U., 1994. Propagation and transport properties dipolar vortices on a γ-plane. Phys. Fluids 6 (10), 3341–3352.
Velasco Fuentes, O.U., van Heijst, G.J.F., Cremers, B., 1995. Chaotic advection by dipolar vortices on a β-plane. J. Fluid Mech. 191, 139–161.
Verron, J., 1986. Topographic eddies in temporally varying oceanic flows. Geophys. Astrophys. Fluid Dyn. 35, 257–276.
Vilela, R.D., de Moura, A.P.S., Grebory, C., 2006. Finite-size effects on open chaotic advection. Phys. Rev. E 73, 026302-1–026302-6.
Wåhlin, A.K., 2004. Topographic advection of dense bottom water. J. Fluid Mech. 510, 95–104.
Waseda, T., Mitsudera, H., 2002. Chaotic advection of the shallow Kuroshio coastal waters. J. Oceanogr. 58 (5), 627–638.
Welander, P., 1955. Studies of the general development of motion in a two-dimensional, ideal fluid. Tellus 7 (2), 141–156.
Wiggins, S., 2005. The dynamical systems approach to Lagrangian transport in oceanic flows. Annu. Rev. Fluid Mech. 37, 295–328.
Yang, H., 1993a. Dependence of Hamiltonian chaos on perturbation structure. Int. J. Bifurc. Chaos 3 (4), 1013–1028.
Yang, H., 1993b. Chaotic mixing and transport in wave systems and atmosphere. Int. J. Bifurc. Chaos 3 (6), 1423–1445.
Yang, H., 1996a. Chaotic transport and mixing by ocean gyre circulation. In: Adler, J., Muller, P., Rozovskii, B. (Eds.), Stochastic modeling in physical oceanography. Boston, Birkhauser, pp. 439–466.
Yang, H., 1996b. The subtropical/subpolar gyre exchange in the presence of annually migrating wind and meandering jet: water mass exchange. J. Phys. Oceanogr. 26 (1), 115–139.
Yang, H., 1996c. Lagrangian modeling of potential vorticity homogenization and the associated front in the Gulf Stream. J. Phys. Oceanogr. 26 (11), 2480–2496.
Yang, H., 1998. The central barrier, asymmetry and random phase in chaotic transport and mixing by Rossby waves in a jet. Int. J. Bifurc. Chaos 8 (6), 1131–1152.
Yang, H., Liu, Z., 1994. Chaotic transport in a double gyre ocean. Geophys. Res. Lett. 21, 545–548.
Yang, H., Liu, Z., 1997. The three-dimensional chaotic transport and the great ocean barrier. J. Phys. Oceanogr. 27 (7), 1258–1273.
Yatsuyanagi, Y., Hatori, T., Kato, T., 2001. Chaotic reconnection due to fast mixing of vortex-current filaments. Earth Planets Space 53, 615–618.
Yuan, G.-C., Pratt, L.J., Jones, C.K.R.T., 2002. Barrier destruction and Lagrangian predictability at depth in a meandering jet. Dyn. Atmos. Oceans. 35 (1), 41–61.
Zaslavsky, G.M., 2007. The Physics of Chaos in Hamiltonian Systems, second ed., Imperial College Press, London, 315p.
Zeng, X., Pielke, R.A., Eykholt, R., 1993. Chaos theory and its applications to the atmosphere. Bull. Amer. Meteorol. Soc. 74 (4), 631–644.
Zyryanov, V.N., 1985. Theory of stationary oceanic currents. Gidrometeoizdat, Leningrad, 248p.
Zyryanov, V.N., 1995. Topographic eddies in the theory of sea currents. Institute of Water Problems of RAS, Moscow, 240p.
Zyryanov, V.N., 2006. Topographic eddies in a stratified ocean. Reg. Chaot. Dyn. 11 (4), 491–521.